



universität
wien

DIPLOMARBEIT

Titel der Diplomarbeit

Thermoelectricity of Inverse Clathrates

Verfasser

Matthias Falmbigl

angestrebter akademischer Grad

Magister der Naturwissenschaften (Mag. rer. nat.)

Wien, 2008

Studienkennzahl lt. Studienblatt:

A 419

Studienrichtung lt. Studienblatt:

CHEMIE

Betreuerin / Betreuer:

Univ. Prof. Dr. Peter Franz Rogl

Abstract

Although Menke and von Schnering already in 1973 synthesised the first compounds, which can be assigned to the group of inverse semiconducting clathrates, so far about only 30 different compounds of this kind are known. In the recent 10 years the interest of research increased, due to the, for thermoelectric applications promising, physical properties. In fact a low thermal conductivity and a rather high electrical conductivity at a high Seebeck-coefficient are to be provided.

Clathrate-compounds could fulfil these requirements, which are in principle rather difficult to combine, because of their structural features. The guest atoms incorporated into the host framework don't form covalent bonds to the other atoms and thus decrease significantly the thermal conductivity by "rattling" i.e. by scattering the heat carrying phonons. A manifold of various atoms can build up the framework and furthermore the physical properties can be shifted into the desired direction by performing specific chemical substitutions.

In this diploma work at first the already known compound $\text{Sn}_{19.3}\text{Cu}_{4.7}\text{P}_{22}\text{I}_8$ was synthesised. To get samples of a proper shape for the measurement of physical properties, an alternative two-step method, containing as a first step mechanical alloying using a ball mill and as a second step hot pressing, was performed. After an optimisation of the initial weighing of the starting materials as well as an optimisation of various parameters in the synthesis steps the specimen was available in a suitable compact shape. The physical properties, which are decisive for thermoelectric applications, namely electrical resistivity, thermal conductivity and Seebeck-coefficient were investigated. The results confirmed semiconducting properties in line with the Zintl-concept. To modify these properties various substitutions in the host-framework were performed. The exchange of Cu by Zn caused a shift of the electrical resistivity to lower values. The measurement of thermal conductivity confirmed that the values like expected don't exceed a sector typical for glass-like behaviour. The determination of lattice parameters using an internal standard as well as the Rietveld-refinement confirmed the successful synthesis of these new compounds.

The measured data for these compounds, due to their high electrical resistivity, don't yet allow a thermoelectric application. Thus further substitutions were performed. For the first time we tried to incorporate silver and gold into the host-framework of inverse clathrates. In this case as well the achievement of this attempt was confirmed by the determination of the lattice parameters as well as the results of the refinement of the structural data. The electrical resistivity of these new compounds exhibited values lowered by a factor of 10^2 at room temperature, whereas at the same time the Seebeck-coefficients were lowered only marginally. Although this significant change in physical properties was reached via a rather small exchange of atoms in the compound, the silver- and gold-containing samples need further improvement of their constitution to get interesting for industrial use.

Furthermore for the first time the measurement of the shear modulus of the compound $\text{Sn}_{19.3}\text{Cu}_{4.7}\text{P}_{22}\text{I}_8$ was performed, which provided the first data on elastic properties of inverse clathrates.

Kurzfassung

Obwohl bereits 1973 durch Menke und von Schnering die ersten Verbindungen, die man der Gruppe der inversen Clathrate zuordnen kann, hergestellt wurden, sind bis heute erst um die 30 Verbindungen dieser Art bekannt. Erst in den letzten 10 Jahren stieg das Interesse der Forschung an diesen Verbindungen, bedingt durch die für thermoelektrische Anwendungen vielversprechenden physikalischen Eigenschaften, stark an. Um für thermoelektrische Anwendungen interessant zu sein, sollten die Materialien eine niedrige thermische Leitfähigkeit, aber gleichzeitig eine gute elektrische Leitfähigkeit bei hohem Seebeck-Koeffizienten aufweisen.

Clathrat-Verbindungen könnten diese Bedingungen, die eigentlich schwer kombinierbar sind, erfüllen, da bedingt durch die in dem Gitter befindlichen Gastatome, die keine kovalenten Bindungen zu den anderen Atomen ausbilden, die Wärmeleitung über Phononen stark eingeschränkt wird. Das Netzwerk kann durch eine Vielzahl verschiedener Atome gebildet werden und durch gezielte Substitutionen sollte eine Beeinflussung der physikalischen Eigenschaften in die gewünschte Richtung möglich sein.

In dieser Arbeit wurde zunächst die schon bekannte Verbindung $\text{Sn}_{19,3}\text{Cu}_{4,7}\text{P}_{22}\text{I}_8$ synthetisiert. Um diese Verbindung der Messung physikalischer Eigenschaften zugänglich zu machen, wurde eine alternative zweistufige Methode verwendet, die im ersten Schritt mechanisches Legieren in einer Kugelmühle und im zweiten Schritt Heißpressen beinhaltet. Nach einer Optimierung sowohl der Einwaage der Ausgangsstoffe als auch der verschiedenen Parameter in den Syntheseschritten stand die Verbindung in einer für die Messungen geeigneten kompakten Form zur Verfügung. Die für die thermoelektrische Anwendung entscheidenden physikalischen Eigenschaften, elektrischer Widerstand, thermische Leitfähigkeit und Seebeck-Koeffizient wurden untersucht. Die Resultate bestätigten die durch das Zintl-Konzept vorhergesagten halbleitenden Eigenschaften. Um eine Verbesserung dieser Eigenschaften zu erzielen (vornehmlich Herabsetzen des elektrischen Widerstandes) wurden verschiedene Substitutionen im Gitter versucht. Der Austausch von Cu durch Zn zeigte eine Verschiebung des elektrischen Widerstandes zu niedrigeren Werten. Die Messung der thermischen Leitfähigkeit zeigte die für diesen Verbindungstyp erwarteten niedrigen Werte. Die Bestimmung der Gitterkonstante mittels internem Standard und die Rietveldverfeinerung der Strukturparameter bestätigte die erfolgreiche Synthese dieser neuen Verbindungen.

Da allerdings die erhaltenen Daten keine Anwendung als thermoelektrisches Material zulassen, weil der elektrische Widerstand noch zu hoch ist, wurden weitere Substitutionen durchgeführt. Erstmals wurde versucht Silber und Gold in das Wirtsgitter eines inversen Clathrates einzubauen. Auch hier konnte der Erfolg dieses Versuches durch Bestimmung der Gitterparameter und Verfeinerung der Röntgendaten bestätigt werden. Der elektrische Widerstand bei Raumtemperatur konnte um den Faktor 10^2 verringert werden, wobei der hohe Seebeck-Koeffizient beibehalten werden konnte. Obwohl hier durch das geringe Ausmaß der substituierten Atome bereits ein großer Effekt auf die physikalischen Eigenschaften erzielt wurde, benötigen auch die hergestellten Silber- und Gold-Verbindungen eine weitere Verbesserung, um für industrielle Anwendungen interessant zu werden.

Weiters wurde erstmals eine Messung des Schermoduls der Verbindung $\text{Sn}_{19,3}\text{Cu}_{4,7}\text{P}_{22}\text{I}_8$ durchgeführt, was die ersten Daten für die elastischen Eigenschaften inverser Clathrate lieferte.

Table of Contents

| | |
|------------------------|-----|
| ABSTRACT | iii |
| KURZFASSUNG | v |
| TABLE OF CONTENTS..... | vii |
| INTRODUCTION..... | 1 |

CHAPTERS

| | |
|---|----|
| 1. Inverse Semiconducting Clathrates | 5 |
| 1.1 Synthesis of Inverse Clathrates | 7 |
| 1.2 Structure of Inverse Type-I-Clathrates | 8 |
| 1.2.1 Crystal Structure of the Compound $\text{Sn}_{19.3}\text{Cu}_{4.7}\text{P}_{22}\text{I}_8$ | 9 |
| 2. Experimental Techniques | 10 |
| 2.1 Furnaces | 10 |
| 2.2 Ball Mill | 11 |
| 2.3 Hot Press | 12 |
| 2.4 X-ray Powder Diffraction – Guinier Technique | 14 |
| 2.4.1 Determination of Lattice Parameters using an Internal Standard | 16 |
| 2.4.2 Refinement of Crystal Structures: The Rietveld-Method | 18 |
| 2.5 Measurement of Electrical Resistivity | 18 |
| 2.5.1 Setup for Low Temperature Measurement | 19 |
| 2.5.2 Setup for High Temperature Measurement | 20 |
| 2.6 Measurement of Thermopower | 21 |
| 2.7 Simultaneous Measurement of Thermopower and Electrical Resistivity | 23 |
| 2.8 Measurement of Thermal Conductivity | 24 |
| 2.9 Measurement of the Shear Modulus | 26 |
| 3. Results and Discussion | 27 |
| 3.1 Synthesis and Structure of Clathrate Compounds | 27 |
| 3.1.1 Synthesis of $\text{Sn}_{19.3}\text{Cu}_{4.7}\text{P}_{22}\text{I}_8$ by a Standard Ampoule Procedure | 27 |

| | |
|--|----|
| 3.1.2 Synthesis of $\text{Sn}_{19.3}\text{Cu}_{4.7}\text{P}_{22}\text{I}_8$ by Ball Milling and Hot Pressing | 27 |
| 3.1.3 Synthesis and Structure of new Clathrate-I-Compounds..... | 31 |
| 3.2 Thermoelectric Performance | 37 |
| 3.2.1 Substitutions in the Clathrate Framework | 38 |
| 3.2.2 Electrical Resistivity | 38 |
| 3.2.3 Seebeck-Coefficient | 45 |
| 3.2.4 Thermal Conductivity | 48 |
| 3.2.5 ZT-Figure of Merit | 50 |
| 3.3 Mechanical Properties | 52 |
| 4. Conclusion | 54 |
| REFERENCES | 55 |
| ACKNOWLEDGEMENTS | 58 |
| CURRICULUM VITAE | 59 |

Introduction

The content of this diploma work is dedicated on the one hand to the synthesis of inverse or polycationic semiconducting Sn-containing clathrates and on the other hand to the investigation and improvement of their thermoelectric properties.

The first clathrate, a chlorine hydrate, was synthesised by Davy in 1811. Powell solved the crystal structure of this compound in 1948. Over many years only gas hydrates and compounds based on hydroquinone and urea were assigned to clathrates. These inclusion compounds have attracted some interest from researchers because of their uncommon structure. Since the 1960s firstly silicates and silicides and later also germanides and stannides that are isostructural to the gas hydrates aroused some interest. All these compounds belong to the polyanionic semiconducting clathrates. Menke and von Schnering [1] were the first to synthesise polycationic clathrates. They found the compound $\text{Ge}_{38}\text{P}_8\text{I}_8$ in their attempt to investigate transport reactions in the Ge-P-system with iodine as a transport agent. The first tin-containing polycationic clathrate-I-structures were reported by Shatruk et al. [3].

Since Thomas Johann Seebeck back in 1821 and Charles Athanase Peltier in 1834 discovered the thermoelectric effects many researchers tried to find new materials for thermoelectric refrigeration and power generation. In order to get a high efficiency the dimensionless thermoelectric figure-of-merit (ZT) should reach high values:

$$(1) \quad Z \cdot T = \frac{T \cdot S^2}{\kappa \cdot \rho}$$

A good thermoelectric material should possess low electrical resistivity ρ , low thermal conductivity κ and have a high Seebeck-coefficient S . A combination of such properties is rare and nature doesn't favour such a combination. To obtain a high efficiency the ZT value should exceed 1, which is not achieved by "classical" thermoelectric materials based on bismuth and lead tellurides.

For the design of fundamentally new thermoelectric materials the Phonon Glass-Electron Crystal (PGEC) concept developed by Slack is of great importance. According to this idea, an effective thermoelectric material should be sought among substances that (i) maintain sufficiently good electrical conductivity but (ii) should contain weakly bound atoms or molecules, which via their "rattling modes" efficiently scatter phonons thus decreasing thermal conductivity.

The first results concerning the thermoelectric properties of the intermetallic clathrates confirmed that these compounds could fulfil these requirements. This stimulated interest in the semiconducting clathrates, as evidenced by a sharply increasing number of publications in the recent years. Especially compounds with clathrate-I-structure show promising thermoelectric properties. It is believed that clathrates offer a wide range of tuning the electronic structure and, correspondingly, properties by performing various substitutions in the framework or regulating the concentration of vacancies [17].

Up to now there have been successful efforts to substitute the group 14 elements in inverse clathrates partially by P, As, Sb, Ga, Te, I, In, Zn, Cd, Cu [18]. In recent years

various studies have shown that Sn-containing inverse clathrates derive from an ideal vacancy-free composition $\text{Sn}_{24}\text{A}_{22}\text{X}_8$ ($\text{A} = \text{P}, \text{As}, \text{Sb}$; $\text{X} = \text{I}, \text{Br}, \text{Cl}, \text{Te}$), which may exhibit vacancies in the framework at the pnictide position [3, 12] as well as at the Sn-position [13].

Nevertheless for many of the up to now synthesised inverse clathrates the thermoelectric properties (S , κ , ρ) have not been investigated so far as can be seen from the table below.

In the present diploma thesis we focused on the compound $\text{Sn}_{19.3}\text{Cu}_{4.7}\text{P}_{22}\text{I}_8$ [15] with the aims (i) to find a simple procedure for synthesis, (ii) to investigate the thermoelectric properties and (iii) to optimise the thermoelectric performance via substitution of Cu and Sn by other suitable elements.

Table 1: Overview on inverse type-I clathrate compounds, structural and physical property data (σ ...electrical conductivity, S ...Seebeck-coefficient, κ ...thermal conductivity, ZT ...figure of merit)

| Compound | Structure Type | Lattice par. | S | σ | κ | ZT | ref. |
|------------------------------|----------------|----------------|-----------------------|--------------------|--------------------|-------------|------|
| | Space group | $[10^{-10}m]$ | $[\mu V/K]$ (300K) | $[S/m]$ (300K) | $[W/mK]$ (300K) | | |
| $Ge_{38}P_8I_8$ | | | | 1,11-6,25 | | | 1 |
| $Ge_{38}As_8I_8$ | $Pm\bar{3}n$ | $a=10.6158(4)$ | | 0,02-0,008; 100 | | | 1,2 |
| $Sn_{24}P_{19.3}I_8$ | $Pm\bar{3}n$ | $a=10.9540(9)$ | 80 | 1500 | 1,8 | 0.02 (300K) | 3,12 |
| $Sn_{24}As_{19.3}I_8$ | unsolved | $a=22.179(1)$ | | | | | 3 |
| $Sn_{10}In_{14}P_{22}I_8$ | $Pm\bar{3}n$ | $a=11.0450(7)$ | | | | | 4 |
| $Sn_{14}In_{10}P_{21.2}I_8$ | $P4_2/m$ | $a=24.745(3)$ | | | | | 4 |
| | | $c=11.067(1)$ | | | | | 4 |
| $I_8Si_{46-x}I_x$ | $Pm\bar{3}n$ | $a=10.4195(7)$ | | | | | 5 |
| $Sn_{24}P_{19.3}Br_xI_{8-x}$ | | | | | | | 6 |
| $x=8$ | $Pm\bar{3}n$ | $a=10.8142(7)$ | | | | | 6 |
| $Sn_{20}Zn_4P_{22-x}I_8$ | $Pm\bar{3}n$ | $a=10.881(1)$ | | | | | 7 |
| $Sn_{17}Zn_7P_{22}I_8$ | $Pm\bar{3}n$ | $a=10.8425(6)$ | | 0,25 | | | 7 |
| $Sn_{17}Zn_7P_{22}Br_8$ | $Pm\bar{3}n$ | $a=10.7254(2)$ | | 250 | | | 7 |
| $Ge_{38}Sb_8I_8$ | $Pm\bar{3}n$ | $a=10.8892(2)$ | -800 | 0,00002; 0,001 | 1,15 | | 1,8 |
| $Sn_{38}Sb_8I_8$ | $Pm\bar{3}n$ | $a=12.0447(3)$ | -600 | 0,1 | 0,7 | | 8 |
| $Ge_{30}P_{16}Te_8$ | $Pm\bar{3}n$ | $a=10.3376(2)$ | 750 | 3,16 | 0,86 | | 9 |
| $Si_{46-x}P_xTe_8$ | | | | | | | 10 |
| $Si_{30}P_{16}Te_8$ | $Pm\bar{3}n$ | $a=9.96457(9)$ | | | | | 10 |
| $x=11$ | | | 60 | 50000 | | | 10 |
| $x=12$ | | | 90 | 30000 | | | 10 |
| $x=13$ | | | 135 | 6000 | 3,9 | 0.45 (900K) | 10 |
| $x=14$ | | | 210 | 1000 | | | 10 |
| $x=15$ | | | 220 | 300 | | | 10 |
| $x=16$ | | | -10 | 0,158 | 4,4 | | 10 |
| $x=17$ | | | 250 (500K) | 0,0158 | | 0.06 (900K) | 10 |
| $Si_{46-x}P_xTe_y$ | $Pm\bar{3}$ | | | | | | 11 |
| $P_{14.7}Si_{31.3}Te_{7.35}$ | $Pm\bar{3}$ | $a=9.9702(3)$ | | | | | 11 |
| $P_{13.6}Si_{32.4}Te_{6.98}$ | $Pm\bar{3}$ | $a=9.9794(2)$ | | | | | 11 |
| $P_{13.0}Si_{33.0}Te_{6.88}$ | $Pm\bar{3}$ | $a=9.9808(2)$ | | | | | 11 |

| Compound | Structure Type | Lattice par. | S | σ | κ | ZT | ref. |
|-------------------------------|---------------------|---------------|-----------------------|-------------------|--------------------|----------------|--------|
| | Space group | $[10^{-10}m]$ | $[\mu V/K]$ (300K) | $[S/m]$ (300K) | $[W/mK]$ (300K) | | |
| $Sn_{24}P_{19.3}Br_xI_{8-x}$ | $Pm\bar{3}n$ | | | | | | 12 |
| x=0 | | | 80 | 1500 | 1,75 | 0.02 (300K) | 12, 13 |
| x=2 | | | | 1340 | 0,5 | | 12 |
| x=3 | | | | 545 | | | 12 |
| x=7 | | | | 405 | | | 12 |
| x=8 | | | 180 | 334 | | | 12 |
| $Sn_{24}P_{19.3}Cl_yI_{8-y}$ | $Pm\bar{3}n$ | | | | | | 12 |
| y=0 | $Pm\bar{3}n$ | a=10.954(1) | | | | | 12 |
| y=0.8 | $Pm\bar{3}n$ | a=10.933(1) | | | | | 12 |
| $Sn_{20.5}As_{22}I_8$ | $Pm\bar{3}n$ | a=11.092(1) | -180 | 0,95 | 0,5 | 0.00002 (300K) | 13 |
| | F23/ $Fm\bar{3}$ | a=22.1837(4) | | | | | 13 |
| $Sn_{19.3}Cu_{4.7}As_{22}I_8$ | $Pm\bar{3}n$ | a=11.1736(3) | | | | | 14 |
| $Sn_{19.3}Cu_{4.7}P_{22}I_8$ | $Pm\bar{3}n$ | a=10.847(1) | | | | | 15 |
| $Ge_{40.0}Te_{5.3}I_8$ | $Pm\bar{3}n$ | a=10.815(1) | | | | | 16 |

1. Inverse Semiconducting Clathrates

Clathrates (from Latin *clatratus* = encaged) are defined as inclusion complexes in which molecules of one substance or atoms are completely enclosed in cavities formed by the framework of another substance. The guest molecules or atoms are captured in the voids of the host crystal structure during formation and are unable to escape until the framework is decomposed. In many cases the crystal lattice of the hosts cannot exist in the absence of the guest. The ratio of the cavity sizes in the host framework to the size of the guest molecules or atoms plays a decisive role in the formation of a clathrate structure. Besides, guests in semiconducting clathrates are always monoatomic.

The clathrate hydrates of gases and liquids crystallise in seven structural types, which are distinguished from each other by Roman numbers (I-VII). It was found that intermetallic clathrates only crystallise in clathrate types I, II, III, VIII and IX. The vast majority of the so far reported clathrates were found to be of the type-I-structure. All these structures can be described by various combinations of polyhedra, forming the structure of the framework with the hosts located in the framework cavities. For a recent survey on clathrates see [22].

The intermetallic clathrates can be classified according to the formal charge of the framework. In the polyanionic compounds the cations (guests) such as alkali, alkaline-earth metals, or europium are trapped in the anionic host framework based on four-bonded group 14 elements (Si, Ge, Sn). But there exist a number of clathrate-I-type compounds characterised by the inverted host-guest polarity. Their framework is built up of group 14 and pnictogen atoms. In the cavities of these structures halogen anions (Cl, Br, I) or Te are enclosed as guests. The framework bears a positive charge and so these compounds are referred to polycationic or inverse clathrates. The majority of the semiconducting clathrates are narrow-gap semiconductors and, in general, Zintl phases [27]. These are characterised by the strict correspondence between the crystal structure and the electronic structure. Classical Zintl phases are binary and ternary compounds, which contain alkali and alkaline-earth metals as cations and main-group elements from groups 13-15 as anions and have structures of any complexity. In such compounds the cation donates electrons to the anion to form a closed-shell electronic configuration. Thus all bonding and non-bonding states in the covalent anionic sublattice are filled, whereas all antibonding states stay vacant [26].

Using the Zintl formalism the composition of an inverse semiconducting clathrate can be easily calculated. For the polycationic tin phosphide halide clathrate the ideal formula would be $\text{Sn}_{24}\text{A}_{22}\text{X}_8$ ($\text{A} = \text{P, As, Sb}$; $\text{X} = \text{I, Br, Cl, Te}$). Since every pnictide atom donates one excess electron, while the halogen atoms in total require 8 electrons to acquire a closed shell, $22 - 8 = 14$ electrons are left. Therefore compensation by formation of vacancies in the pnictogen positions or the tin positions is observed. The removal of one pnictide atom compensates five electrons, the removal of one Sn-atom compensates four electrons. The composition of the resulting compound can be calculated by the following formula:

$$(2) \quad y = \frac{14}{x}$$

With $x = 4$ for $\text{Sn}_{24-y}\text{A}_{22}\text{X}_8$ thus $y = 3.5$. A sample, which exactly follows this prediction, is $\text{Sn}_{20.5}\text{As}_{22}\text{I}_8$ [13]. With $x = 5$ for $\text{Sn}_{24}\text{A}_{22-y}\text{X}_8$ $y = 2.8$. A few samples with this composition were reported in [3, 6, 12].

Another option to compensate the remaining electrons is the hetero-valent substitution of the Sn-atoms by metal atoms with a smaller number of valence electrons ($14-z$ where z is the group number in the periodic table). To prepare the vacancy-free compound $\text{Sn}_{24-x}\text{M}_x\text{P}_{22}\text{I}_8$ the total number of metal atoms x can be calculated with the formula:

$$(3) \quad x = \frac{14}{14 - z}$$

Moreover the 14 electrons can be compensated simultaneously by hetero-valent substitution and vacancy formation in the pnictogen position. The two coefficients x and y in the general formula $\text{Sn}_{24-x}\text{M}_x\text{P}_{22-y}\text{I}_8$ are then related by the equation:

$$(4) \quad x \cdot (14 - z) + 5 \cdot y = 14$$

One of many examples for this case is the composition $\text{Sn}_{14}\text{In}_{10}\text{P}_{21.2}\text{I}_8$.

But in the group of clathrate compounds a second group can be distinguished, which lies beyond the scope of the Zintl formalism. The compounds involved are characterised by their vacancy free structures. This type of structure is exhibited for example by silicides. The electrons are not compensated and so they occupy the antibonding conduction band of the host framework. Therefore these Si-compounds should exhibit metallic properties. This deviation of the Zintl formalism only appears when the cleavage of the bonds of the framework atoms is energetically less favourable than the filling of the conduction band. Also the tin arsenide iodide $\text{Sn}_{17.6}\text{Cu}_{6.4}\text{As}_{22}\text{I}_8$ does not satisfy the Zintl principle, but the references for this compound are contrary to each other. In the review [18], published in 2004, this compound is presented as an example for deviations of the Zintl formalism, but in [14], published in 2005, the same author points out, that all attempts synthesising a sample with the composition $\text{Sn}_{24-x}\text{Cu}_x\text{As}_{22}\text{I}_8$ where $x > 4.7$ were unsuccessful. The reasons for the deviation stay unclear. Maybe also in this case the vacancy formation is energetically less favourable than filling the antibonding states with excess electrons.

1.1 Synthesis of Inverse Clathrates

Only a few routes for synthesis of semiconducting polycationic clathrates have been reported so far in literature. The first inverse clathrates with the general structure $\text{Ge}_{38}\text{A}_8\text{X}_8$ ($\text{A} = \text{P}, \text{As}, \text{Sb}$ and $\text{X} = \text{Cl}, \text{Br}, \text{I}$) were synthesised by Menke and von Schnering [1] reacting stoichiometric amounts of the elements or halogenides, sealed in evacuated quartz glass ampoules at temperatures of 600-1000 °C. To get single crystals they reported that it is useful to set a temperature gradient of 50-100 °C. The reaction products formed within a few days at the cold end of the silica tube. With the exception of $\text{Sn}_{38}\text{Sb}_8\text{I}_8$ [8] all polycationic clathrates containing Sn as group 14 element in the framework were synthesised by a two-step ampoule technique. The stoichiometric mixtures of the powders of the elements and Sn-halogenides were sealed in evacuated quartz glass ampoules and heat treated for several days, reground and subjected to a second annealing ($T \leq 500$ °C). Suitable single crystals for x-ray structure determination were taken if possible after the first step of annealing. In some cases a chemical transport reaction was performed for this purpose. Sometimes storage and preparation of the starting materials was carried out in argon-filled glove boxes [11, 13]. For the synthesis of the clathrate compound $\text{I}_8\text{Si}_{46-x}\text{I}_x$ Reny reported a high pressure and high temperature technique (HPHT) [5]. A stoichiometric mixture of the elements Si and I was ground and the resulting powder was placed in an h-BN cell, which was in turn placed in a carbon tube heater and in a pyrophyllite cube as a pressure media. A cubic multi-anvil press was used. The BN cell was heated electrically by the carbon heater while the temperature was monitored by a Pt/PtRh-thermocouple placed under the cell. The pressure and temperature applied on the sample were respectively 5 GPa and 700 °C for 1 hour. Surprisingly they found that an addition of only 1 % of the clathrate compound to the starting mixtures increased the yield of the clathrate formation from 42 up to 90 mass %.

Kishimoto described another preparation method in a couple of publications [8, 9, 10]. The type I clathrates $\text{Ge}_{38}\text{Sb}_8\text{I}_8$, $\text{Sn}_{38}\text{Sb}_8\text{I}_8$, $\text{Ge}_{30}\text{P}_{16}\text{Te}_8$ and $\text{Si}_{46-x}\text{P}_x\text{Te}_8$ were synthesised using spark plasma sintering (SPS). Raw powder or grains of the elements with grain size below 0.5 mm were pulverised using a planetary mill. The pulverised powder was partially or fully mechanically alloyed and afterwards sintered in a graphite die by SPS carried out at a pressure of 40 MPa in argon of 53.3 kPa. The sintering temperatures were dependent on the sample materials: 873 K ($\text{Ge}_{38}\text{Sb}_8\text{I}_8$, $\text{Ge}_{30}\text{P}_{16}\text{Te}_8$), 638 K ($\text{Sn}_{38}\text{Sb}_8\text{I}_8$) and 1123-1273 K ($\text{Si}_{46-x}\text{P}_x\text{Te}_8$).

1.2 Structure of Inverse Type-I-Clathrates

The clathrate type-I-structure contains two types of polyhedra (Fig. 1), the pentagonal dodecahedron and the larger 14-face tetrakaidecahedron. The pentagonal dodecahedron is a 20-vertex polyhedron containing 12 regular pentagonal faces. The correct notation is $[5^{12}]$. It is a Platonic body, in which all corners are equivalent and all faces are identical. The larger tetrakaidecahedron is formed by 12 pentagonal and 2 hexagonal faces (notation: $[5^{12}6^2]$). These 24-vertex polyhedra are linked to each other by sharing hexagonal faces forming channels through the network, which are not intersecting.

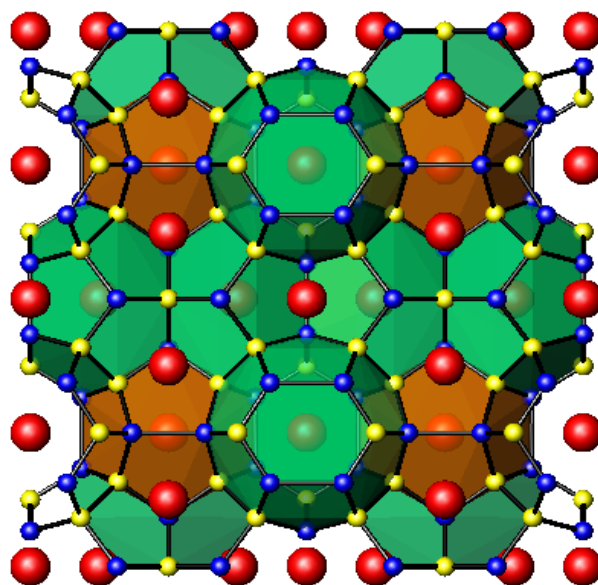


Fig. 1: Two types of polyhedra in the clathrate-I-structure: pentagonal dodecahedra (orange) and tetrakaidecahedra (green)

The pentagonal dodecahedra are enclosed in this system of channels and are isolated from each other. The type-I unit cell contains 46 atoms of the framework and has 2 small and 6 larger cavities. Therefore the general formula is $G_8[E_{46}]$. Structures of type-I generally crystallise in the space group $Pm\bar{3}n$. Although for structures $Ge_{38}A_8X_8$ ($A = P, As, Sb$ and $X = Cl, Br$) the centre of symmetry was claimed to be absent and they all were reported to crystallise in the space group $P\bar{4}3n$ [1], a recent re-determination of the structure of $Ge_{38}Sb_8I_8$ unambiguously revealed centrosymmetry $Pm\bar{3}n$ and thus isotypism with clathrate type-I [23]. Until now one type of superstructures is known for the inverse clathrate-type-I-structure: $Sn_{14}In_{10}P_{21.2}I_8$ crystallises in the tetragonal space group $P4_2/m$. The unit cell volume is increased by a factor of five compared to the unit cell volume of the basic cubic clathrate corresponding to partial ordering of vacancies.

1.2.1 Crystal Structure of the Compound $\text{Sn}_{19.3}\text{Cu}_{4.7}\text{P}_{22}\text{I}_8$

$\text{Sn}_{19.3}\text{Cu}_{4.7}\text{P}_{22}\text{I}_8$ is isotypic with the structure of type-I clathrates crystallising in the centrosymmetric space group $\text{Pm}\bar{3}\text{n}$ (for a standardised setting of the unit cell see TYPIC [20]). According to literature data [15] in the special case of $\text{Sn}_{19.3}\text{Cu}_{4.7}\text{P}_{22}\text{I}_8$ the 24k-position is split into two very close positions, which means there are two possible positions very close to each other and if one of the positions is occupied the other one stays empty. Both positions are occupied by tin as well as by copper in a random fashion. The M1-position is coordinated by 3 P-atoms and one metal-atom. When this position is occupied by a tin-atom, 3 P and another tin-atom at another M1-position surround it, but when copper is occupying an M1-position it forms a metal-metal bond with a copper at the M2-position. Each M2-atom is surrounded by 3 P-atoms and in case of copper by another copper in M1. When the M2-position is occupied by tin it forms only three bonds to phosphorus atoms and is not bonded to other metal atoms. The phosphorus atoms are occupying the 6d(P1) and 16i(P2) position. At the 6d-position the coordination environment consists of 4 metal atoms whereas 3 metal and one P-atom surround P2. The 2a-position of iodine is located in the center of the pentagonal dodecahedron built up by the framework forming Sn and P atoms and the 6c-position in the larger cavity of a tetrakaidecahedron is also occupied by iodine.

The crystal structure (Fig. 2) was drawn with the program ATOMS. The split position at the 24k-position is not shown in the picture. No differentiation was made between Sn and Cu-atoms. The iodine atoms are coloured red. Additionally the iodine atoms in the 6c-position (larger cavities) are shaded. The bonds between tin (blue) and phosphorus (yellow) atoms are displayed by black sticks. To distinguish between the two different phosphorus sites the 6d-positions are also shaded. Three metal atoms and one phosphorus atom surround the P-atoms placed in the 16i-position. P-atoms in the 6d-position are bond to four metal atoms.

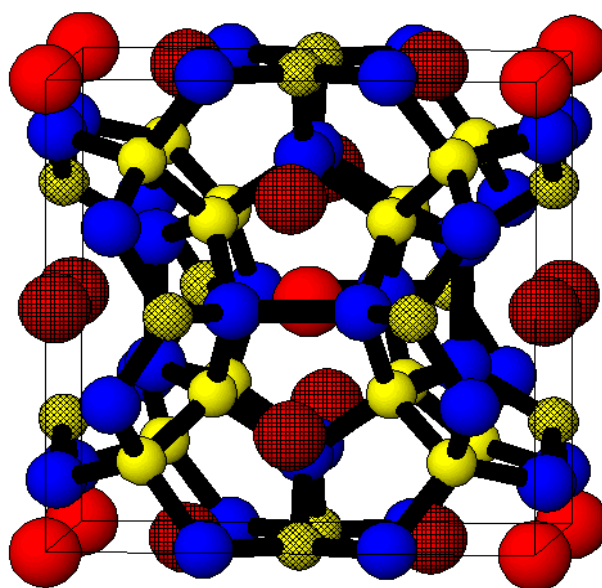


Fig. 2: Unit cell of $\text{Sn}_{19.3}\text{Cu}_{4.7}\text{P}_{22}\text{I}_8$: iodine (red), P (yellow), Sn/Cu (blue)

2. Experimental Techniques

This chapter gives an overview and description of the experimental equipment and techniques used in this work.

2.1 Furnaces

Two tubular constantan-wire wound furnaces (Haereus) with a total length of 60 cm were installed. First of all the electrical resistance was measured by a multimeter, because it was unknown, if the furnaces still work correctly. The one with a tube diameter of 6.5 cm (furnace 1) showed an electrical resistance of $17.0\ \Omega$, the other one with a tube diameter of 5 cm (furnace 2) showed an electrical resistance of $19.2\ \Omega$. The power of the furnaces is 3 kW and the maximum operating temperature is $1100\ ^\circ\text{C}$. For power control two temperature controllers and two thyristors were used and assembled into a computer case. The Thyristor (TE10S, Eurotherm) is a solid-state semiconductor device. For temperature control in case of furnace 1 a Eurotherm 3216 Controller and in case of furnace 2 a Eurotherm 3116 Controller were installed. For wiring standard Cu-wires were used, only the thyristors and the furnaces were connected by $1.5\ \text{mm}^2$ triple core cables.

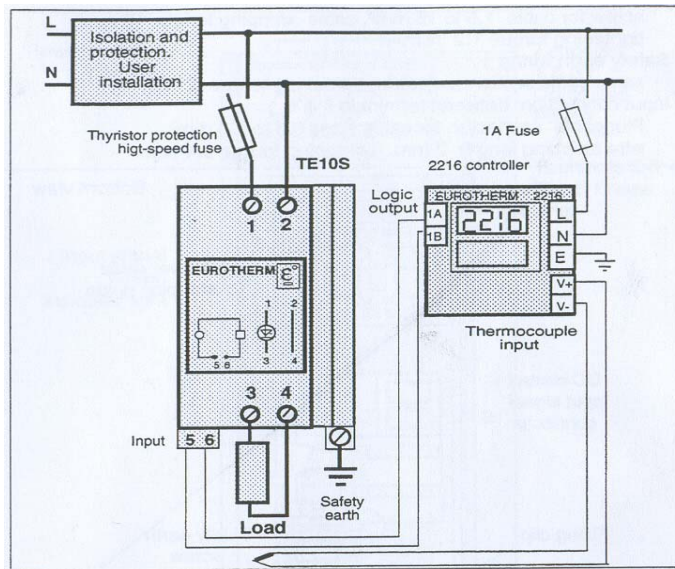


Fig. 3: Connection scheme of the furnaces FM I and FM II [28]

The two systems are running with AC 220 volts. Two S-type thermocouples were assembled for temperature measurement and connected to the controller by correct compensating shielded cables. As explosion protection high-temperature oxidation resistant steel tubes (WNR. 14841, heat resistant in air up to $1150\ ^\circ\text{C}$) with a wall thickness of 3.6 mm (furnace 1) and a wall thickness of 2.6 mm (furnace 2) were incorporated into the middle of the heating zones. Furnace 2 showed overheating of only $1\ ^\circ\text{C}$ at $600\ ^\circ\text{C}$, furnace 1 overheated by $4\ ^\circ\text{C}$ when heated up to $700\ ^\circ\text{C}$.

2.2 Ball Mill

For mechanical alloying a planetary ball mill “Vario Planetenmühle, Pulverisette 4” was used. It is called planetary mill because the vials show a planet-like movement. The crucibles are arranged on a rotating support disk and a special drive mechanism causes them to rotate around their own axes. So there is one centrifugal force produced by the vials rotating around their own axes and another one produced by the rotating support disk. Both centrifugal forces act on the contents of the crucible. Since the vial and the supporting disk rotate in opposite directions, the centrifugal forces alternately act in forward and opposite directions. When the grinding balls run down the inside wall of the crucible they generate a friction effect. This is followed by a free movement of the balls in the inner chamber of the vial and collision against the opposite inside wall, the so-called impact effect (Fig. 4). It is possible to control the main disk and the vial speed independently in a large range. The grinding balls and vials are available in different size and materials like agate, silicon nitride, sintered corundum, zirconia, chrome steel, Cr-Ni steel and tungsten carbide. Usually the balls and crucibles used are of the same material. Possible contaminations by these materials have to be considered. The density of the grinding medium should be high enough to produce a high impact force. In my case steel crucibles with a volume of 45 ml and steel balls with a diameter of 3 mm were used.

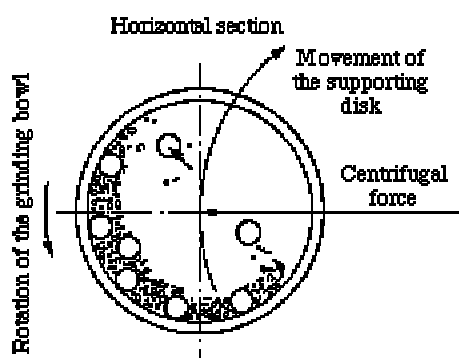


Fig. 4: Centrifugal forces in a planetary mill [29]

There are lots of parameters, which can be varied independently from each other. The size of the balls is an important parameter. Larger balls guarantee a higher impact force, while smaller balls are more favourable for intense frictional action and promote amorphous phase formation. The temperature limits the milling speed. Higher temperature is advantageous for diffusion processes, which are involved in the formation of alloy phases, but the danger of decomposition also increases. The most important parameter is the milling time. Because of the increasing contamination with time the milling time should be kept as short as possible. The ball-to-powder weight ratio (BPR) also has an influence on the process. Most commonly a ratio of 10:1 is used. Alloying occurs due to the impact forces, thus the extent of filling the vials should not be chosen too high, to make sure the balls and powder particles have enough space to move around freely in the milling container. Therefore approximately 50 % of vial space should stay empty. There are a few options to set

the milling atmosphere to avoid contamination by oxidation. The crucibles can be evacuated or filled with inert gases like Argon or Helium. In some cases a Process Control Agent (PCA) is added to the powder to reduce the effect of cold welding. A balance between cold welding and fracturing of particles should always be aspired. Process Control Agents can be solids, liquids or gases. They are mostly, but not necessarily, organic compounds, which act as surface-active agents. The PCA adsorbs at the surface of the particles and minimises cold welding between powder particles and thereby inhibits agglomeration. By adsorption on the particle surfaces the PCA lowers surface tension of the solid materials. This results in the use of shorter milling times and generation of finer powder. The most frequently used Process Control Agents are stearic acids, methanol, ethanol and hexane. An increase of PCA content leads to an exponential decrease of the powder size for a given milling time. In my case cyclohexane was used to reduce oxidation.

2.3 Hot Press

The Hot Press “Heisspresse HP W 200/250-2200-200-KS“ (FCT Systeme GmbH) can be used at a maximum temperature of 2200 °C. The heating power is in the range of 0-40 kW. The furnace is build of high-density graphite. The pressure can be varied from $5.0 \cdot 10^{-2}$ to 1100 mbar. The hydraulic system can create a maximum press capacity of 140 kN. Ar and N₂ can be used as inert gases to prevent the samples from oxidation. A closed cooling water system is used with a back-up system connected to the city-water. The temperature of the cooling water should be lower than 25 °C for sufficient cooling during the working process. For non-contact temperature measurement and regulation a pyrometer with a working range of 400–2500 °C is installed. For measurement of lower temperatures a thermocouple can be installed. A position measuring system is detecting the velocity and degree of densification.



Fig. 5: Hot Press HP W 200/250-2200-200KS [30]

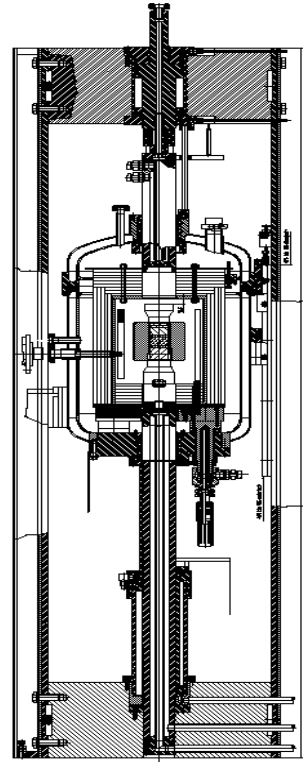


Fig. 6: Cross section through the HotPress [30]

The furnace chamber is made of double-walled steel. In-between the walls the cooling water is circulating. The top cover is fixed and the lower part of the chamber can be moved by a hydraulic system to place the sample into and remove the sample from the chamber.

Unlike solid-state sintering during heating pressure is applied to the sample. The advantages of this procedure are reduction of sintering time and temperature and moreover the porosity of the material is decreased. The mechanisms of the chemical reactions are the same as in the usual sintering process. The materials exchange is driven by diffusion and viscous flow. Most often Hot Pressing is used for synthesis of ceramic materials, because it is the most elegant way to produce ceramic compositions at nearly theoretical density (up to 95 % of theoretical density). With this method, however, only simple shapes can be created. Some limits are set by the die materials, which have to be pressure and heat-resistant. Traditionally graphite dies are used, but graphite must be protected from oxidation and is also a very brittle material. In our case a graphite cylinder with an inner diameter of 10 mm is used. The height of this cylinder is 50 mm. The sample can be filled in as a powder or can be pre-compacted in a metal die. The sample is placed in-between two small slices of graphite. The die is surrounded by some massive graphite parts, which apply the pressure onto the pistil of 10 mm diameter, and align in the chamber.

2.4 X-ray Powder Diffraction – Guinier Technique

X-ray powder diffraction is a powerful method for phase identification in crystalline materials. Furthermore it offers a wide range of additional applications like crystal structure determination, refinement of the structural model, quantitative phase analysis, texture analysis, investigation of domain size, etc.

To generate the required radiation with a wavelength in the range of typical atomic distances of 10^{-10} m an X-ray tube is used. The tube consists of a cathode usually made of tungsten, which can be heated in order to create free electrons by thermionic emission. These electrons are accelerated in an electric field with a typical range of 20-60 kV to the anode. They hit the target, which is also made of tungsten and layered by a thick layer of metals like Cu, Mo, Co or Fe. The characteristic lines depending on the element used are created by the ionisation of core electrons of the target material by the accelerated electrons of the cathode. An electron of an outer orbital drops down to occupy this level. Each metal gives a characteristic X-ray spectrum with element specific wavelengths according to the differences of the energy levels involved in the transition. This transition is only allowed when the difference of the azimuthal quantum number of the states involved is not zero ($\Delta l \neq 0$). The emitted X-ray radiation at characteristic wavelengths due to the unique energy difference of the orbital states is used for powder diffraction. Additionally always the so-called “Bremsstrahlung” is observed stemming from electrons, which hit the sample, enter it and then get decelerated in the electric field of the target atoms, although about 99.5 % of this energy is converted into heat. Thus efficient cooling of the X-ray tube is mandatory. Since there is no limitation, this radiation has energies between 0 and the maximum energy of the electrons (λ_{\min}). The intensity spreading follows the Maxwell-Boltzmann distribution with a maximum at approximately $1.5 \lambda_{\min}$. The nomenclature of characteristic X-ray radiation follows the nomenclature of the atomic shells (K, L, M, ...). For example the transition of 2p to 1s is called K_{α} whereas the radiation created by the transition of 3p to 1s is called K_{β} . An additional splitting into a doublet of, for example, K_{α} into $K_{\alpha 1}$ and $K_{\alpha 2}$ is due to different spin states in the 2p orbital. According to the different occupations of these two spin states the ratio of $K_{\alpha 1}$ to $K_{\alpha 2}$ is 2:1. In most cases the K_{α} radiation of the above-mentioned metals is used for X-ray powder diffraction.

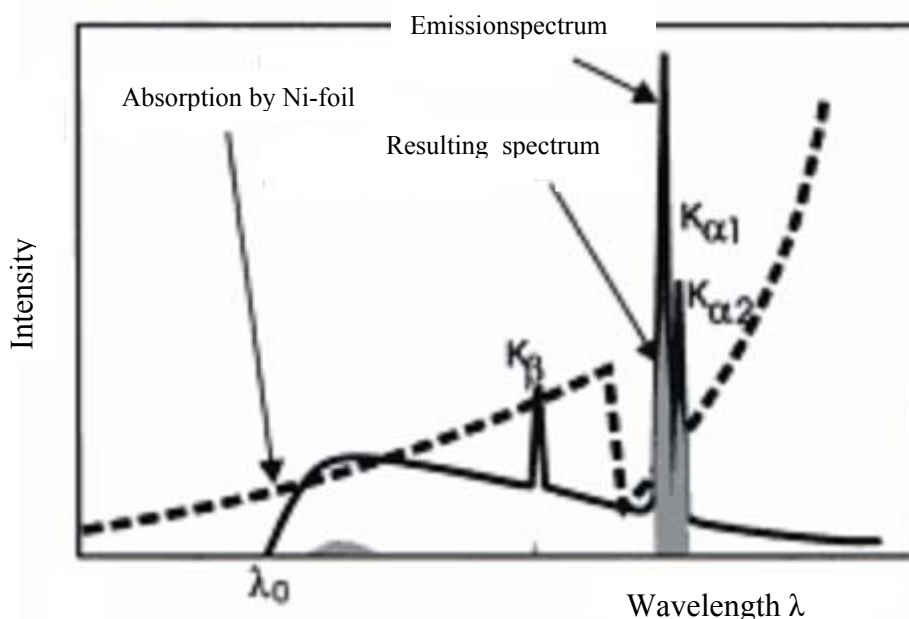


Fig. 7: Bremsstrahlung and characteristic X-ray radiation of Cu and resulting radiation after K_{β} -filtering [31]

In contrast to diffractometers using Bragg-Brentano pseudo-focusing geometry the Guinier technique uses only $K_{\alpha 1}$ -Radiation. In Bragg-Brentano geometry the K_{α} -radiation is separated from the K_{β} -radiation using suitable filter materials (Fig.7). In the Guinier technique the incident beam emitted by the X-ray tube is monochromated and focused by a curved Si- or Ge-single crystal oriented for (111)-reflection, which offers the opportunity to use $K_{\alpha 1}$ -radiation only. To get a parallel beam and to reduce divergence an additional soller slit is used.

The samples need to be in form of fine powders ($<20 \mu\text{m}$). A conventional plastic foil is fixed on the sample holder and some vaseline is smeared over it. Then a thin layer of powder is spread on the top before the sample holder is fixed in a sliding carriage. The detection system used for the scattered X-rays in Guinier technique is an Imaging plate. A flexible plastic plate coated with a $150 \mu\text{m}$ layer of BaFBr:Eu^{2+} in organic binder is used. The BaFBr is doped with Eu^{2+} -ions. These are sensitive to X-ray radiation, which by absorption produces Eu^{3+} and electrons captured in colour centres (step 2, Fig. 8). A two-dimensional image of the intensity is stored. After the measurement the image plate is scanned by a He-Ne-Laser, which stimulates emission from the trapped electrons at 390 nm (step 3, Fig. 8). These photons are detected by photocell via a photomultiplier. The scanning step should be repeated 2-5 times, because not all colour centres are removed at the first scan. A halogen lamp is used for erasure (step 1, Fig. 8). All remaining colour centres at the image plate are removed by exposure with white light. The exposure time is limited to the fact that fading of the colour centres of 25 % after 10 hours is appearing.

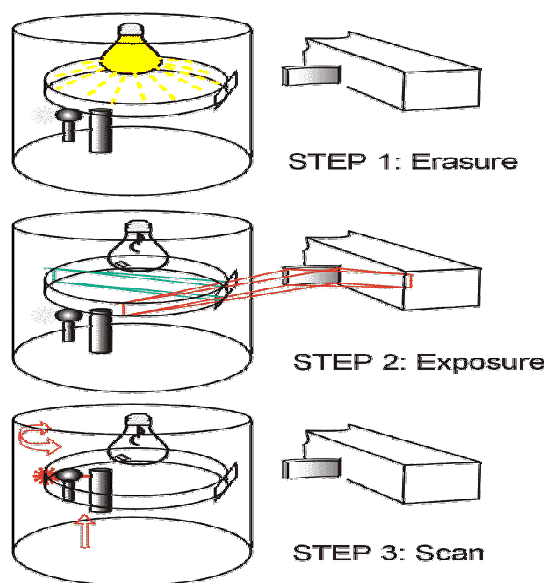


Fig. 8: Imaging plate

An advantage of the Guinier technique is the simultaneous detection of the whole spectrum. The disadvantage of this technique is the distortion of the peak shape (asymmetry) caused by the arrangement of the whole detection system, which might lead to difficulties in the Rietveld-refinement. When the sample produces fluorescence radiation the only way to overcome this problem in the Guinier technique is to change to another wavelength.

The equipment used in my experiments is working with Fe $K_{\alpha 1}$ -Radiation (1.93597 Å). Instead of a Ge-single crystal a quartz-monochromator is used. The measurement of the samples is executed at a voltage of 40 kV and a current of 25 mA. At the image plate the intensities are usually recorded in the range from 8° to 100° in 2θ .

2.4.1 Determination of Lattice Parameters using an Internal Standard

It is a difficult task to formulate a mathematical description dealing with all measurement errors, which contribute to a shift of the reflexes in 2θ . Thus external or internal standards are used to eliminate the total error caused by a manifold of different influences like sample displacement. Substances (Si, Ge ...) with well defined lattice parameters are used as standards. To define a proper correction function for the measured data, the difference of $2\theta_{\text{obs}}$ and $2\theta_{\text{calc}}$ ($\Delta 2\theta$) is plotted versus $2\theta_{\text{obs}}$. Usually a polynomial function of 0^{th} to 4^{th} order is calculated as an approach function.

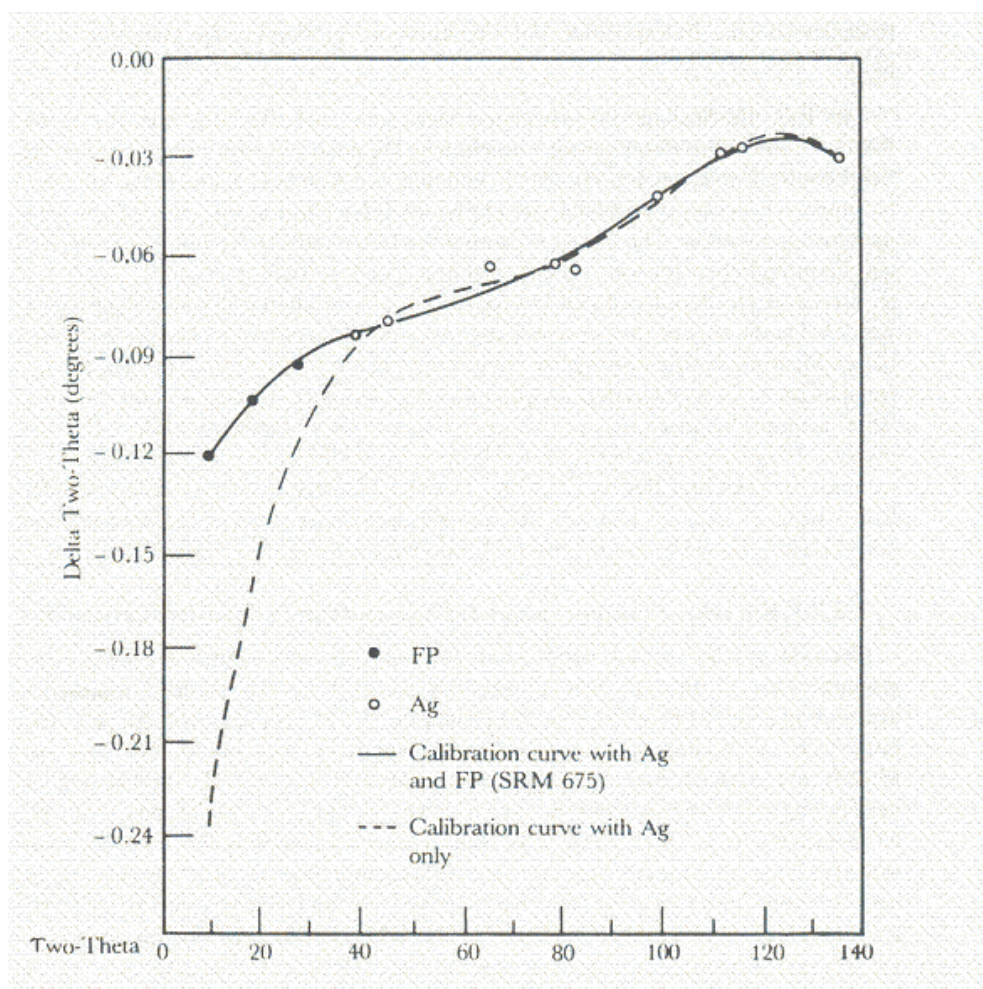


Fig. 9: Polynomial function for the correction of lattice parameters [32]

Extrapolation of this function is problematic and can cause severe mistakes in calculation. Therefore the Bragg-reflections of the sample taken into account for the determination of lattice parameters should be within the first and the last measured peak of the standard substance. For exact measurements of the diffraction angles internal standards should be used, because these are also correcting the sample displacement and errors in transmission of the sample holder. One disadvantage of using internal standards is, that the sample is contaminated and cannot be used for further investigations. To select a suitable standard substance some requirements should be fulfilled. The sample peaks taken for the lattice parameter determination should be in-between the first and the last X-ray reflex of the standard substance as already mentioned. The peaks of the standard and the sample should not overlap and moreover the strongest reflections of sample and standard should show almost the same intensities. For the determination of lattice parameters the PC-program MENU was used.

2.4.2 Refinement of Crystal Structures: The Rietveld-Method

H. M. Rietveld developed in 1967 and 1969 a method for the refinement of the crystal structure information of powder patterns. Initially only for neutron diffraction data, but soon the method was extended also to the higher requirements of X-ray-radiation. In Rietveld-refinement the measured pattern is compared to a theoretical one. The pattern is mathematically described using structure-related, profile-related and instrument-related parameters. All these parameters are refined in a least squares process, usually using a quantity called χ^2 .

$$(5) \quad \chi^2 = \frac{\sum_i w_i \cdot (y_{Oi} - y_{Ci})^2}{\sum_i w_i \cdot y_{Oi}}$$

y_{Oi} is the observed intensity at point i , y_{Ci} is the calculated intensity at point i and w_i is a weight factor.

The refinement requires a starting model giving all relevant structural information. The parameters are refined stepwise and their values have to be controlled after each step in order to avoid physically wrong results. Quality criteria to describe the improvement are the so-called R-values, which are separated into profile and structure R-values. Another very significant quality criterion is the difference curve between observed and calculated pattern, because its shape tells a lot about the reasons for the mismatch.

For all samples the program FullProf [24] with the Windows tool WinPLOTR [25] was used to refine the crystal structures.

2.5 Measurement of Electrical Resistivity

Electrical resistivity of samples was measured in the temperature range of 150 K to 575 K. For the low temperature section (150-300 K) and the high temperature section (300–575 K) two different devices were used. In both cases the electrical resistivity of the samples was measured starting at the lowest temperature in order to get more stable conditions. Furthermore in both devices the resistivity of the samples, which are bar-shaped, is measured using a dc four point technique to eliminate the resistance of the wires. The current is applied using the two outer contacts and the resulting voltage drop is measured between the two inner contacts. The specific resistivity (ρ) of the samples is calculated by the following formula:

$$(6) \quad \rho = \frac{U \cdot A}{I \cdot l}$$

U is the voltage drop, I the applied current, l is the length and A is the cross section.

2.5.1 Setup for Low Temperature Measurement

In this device the contact to the sample is made using four gold needles, which are pressed against the sample by springs (Fig. 10). The equipment offers the possibility to mount two samples at the same time to the holder and measure them in parallel, one with a wider and one with a smaller distance between the gold pins. The current is applied by a Lakeshore Resistance Bridge 370 AC, which in addition measures the voltage and the temperature. The sample temperature is determined using a Pt100. This device can in principal measure temperatures down to 4.2 K. Temperatures below 30 K are then detected with a Ge resistive sensor. The data are sent to a PC, where a program converts and displays them.

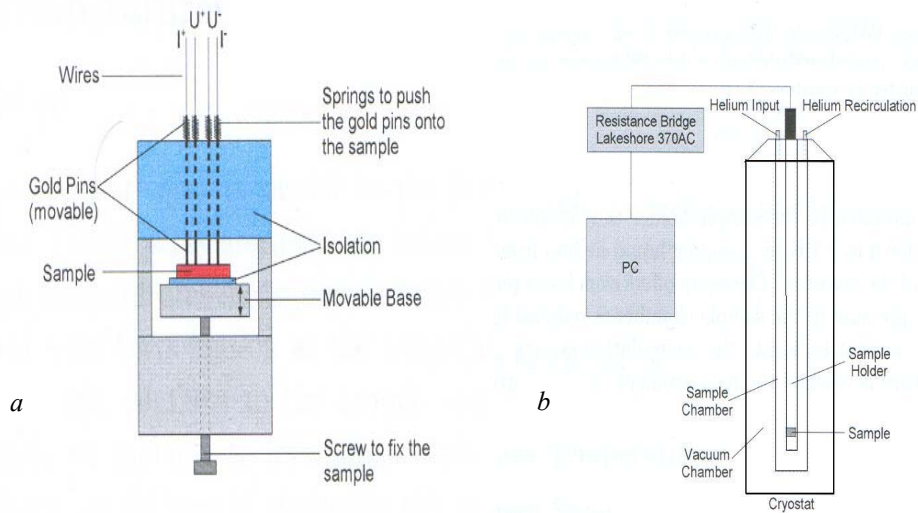


Fig. 10: a shows the sample mounted on the sample holder and b shows the whole measurement station

2. 5. 2 Setup for High Temperature Measurement

Here instead of gold pins and springs, which would lose their tension at higher temperatures, copper wires are used to contact the samples. The wires could not be fixed to the sample by spot-welding because the temperature reached in this case would destroy the clathrate compounds. Thus conduction silver was used for the contact between sample and copper wires. This of course creates two problematic influences on the measurement results. The cross section as well as the tap length diverges from that of the sample and the specific resistivity is influenced by silver. One problem is the deviation from spot-like contacts using silver paste. In this case the contacts are much larger and imprecise in comparison to contacts of welded copper or gold pins. The diffusion of silver into the sample especially at higher temperatures can also lead to some erroneous values during the measurement. To solve the first problem a geometrical correction factor was applied to the high temperature electric resistivity data, which was calculated using the values of the low temperature measurement results at room temperature. The reliability of this correction procedure was proven by F. Röhrbacher (Diplomarbeit) in a comparison using two samples of NBS-steel, one contacted by spot-welding and the other one contacted with conduction silver. However, since the high-temperature measurement curves fit quite well to those at low temperatures concerning the slope at room temperature and as the highest temperature measured did not exceed 450 °C, no correction for the diffusion of silver was applied.

The sample holder offers, as it is the case in the LT-equipment, the opportunity of measuring two samples in one run (Fig. 11). The samples are fixed in-between two mica plates by screws. To contact the copper wires of the sample with the measurement device, they have to be wound around a copper screw, which is then tightened to guarantee a good contact throughout the measurement. The temperature is detected via a Ni-NiCr thermocouple.

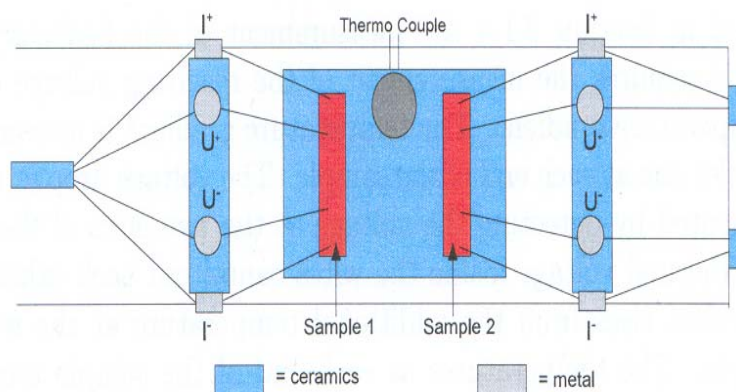


Fig. 11: Sample holder for high temperature measurement

The sample holder is fixed in the steel pipe of the furnace (Naber R70/9). In order to avoid oxidation of the sample or the sample holder the steel pipe can be evacuated

using an oil-diffusion pump (Fig. 12). A constant current is supplied using the two outer contacts by a constant dc-calibrator (Knick J152) and the voltage drop is measured between the inner ones using a nanovoltmeter (Keithley 181). In order to compensate thermo voltages the voltage drop along the samples is measured twice changing the direction of applied current. To calculate the specific resistivity the arithmetic average of both values is used. Since the nanovoltmeter has only one line-in a multi-plexer with gold-coated mechanical contacts (Burster 1630) is used to switch between the different signals. The measured voltages of the sample and the thermocouple are converted by a computer program into a ρ vs. T plot.

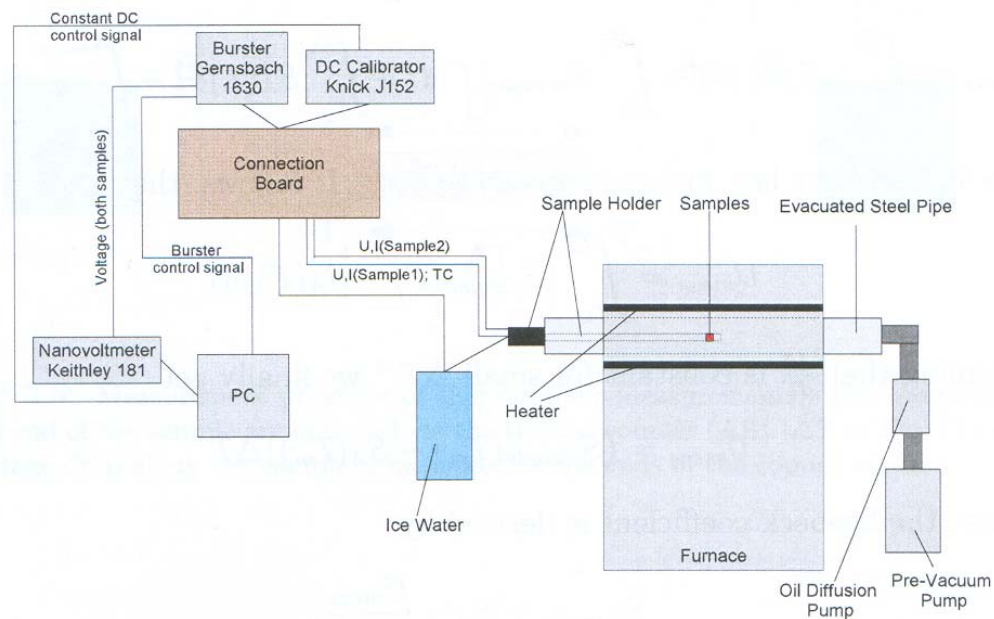


Fig. 12: Measurement station for high temperatures

2.6 Measurement of Thermopower

The thermopower S_x of the samples was measured with a four-point technique using a differential method in terms of seesaw heating. The Seebeck-coefficient was measured in a temperature range of 160-300 K. This device has two strain gauges as heaters, which can raise a temperature gradient in both directions of the usually bar-shaped sample. These strain gauges are glued onto two detached small areas of the sample holder. The sample is fixed on both ends to the heaters using GE-varnish. Then on each end of the sample a Constantan/Chromel thermocouple is contacted to the sample by conduction silver. In principal the contacts can also be soldered using Sn but for my samples this was impossible (Fig. 13). The sample chamber, which is inserted into a He-cryostat, is sealed by an Indium-wire, which is clamped by screws in-between the chamber and its cover to get it vacuum tight. The chamber is

evacuated and a small amount of He(g) is pumped in, to cool down to the desired temperature. A valve, which is controlled by the PC-program, and the two heaters are used to regulate and stabilize the temperature at the measurement points. The valve is connected to an oil-diffusion pump, which is reducing the He(g)-pressure inside the chamber. The temperature is measured with a Pt100 and below 30 K with a Ge resistive sensor. The absolute thermopower of the sample was calculated using the following formula:

$$(7) \quad S_x = S_{Ch} - \frac{V_{Ch}}{V_{Ch} - V_{Co}} (S_{Ch} - S_{Co})$$

Here S_{Ch} and S_{Co} are the absolute thermopowers of Chromel and Constantan, and V_{Ch} and V_{Co} the voltages along the Chromel and Constantan circuit, respectively. During the measurement a small temperature gradient of about 0.2 K is applied to the sample, successively in both directions, which allows eliminating spurious voltages in the measurement circuit.

Due to the relative high electrical resistivity only the measurement of the composition $\text{Sn}_{19.3}\text{Cu}_{1.7}\text{Zn}_3\text{P}_{22}\text{I}_8$ worked out, but even in this case the values show large scatter. The attempt to measure in addition also the thermopower of $\text{Sn}_{19.3}\text{Cu}_{2.7}\text{Zn}_2\text{P}_{22}\text{I}_8$ failed. The values for Seebeck-coefficient show large scatter in the whole temperature range, but at least they are in the expected order of magnitude.

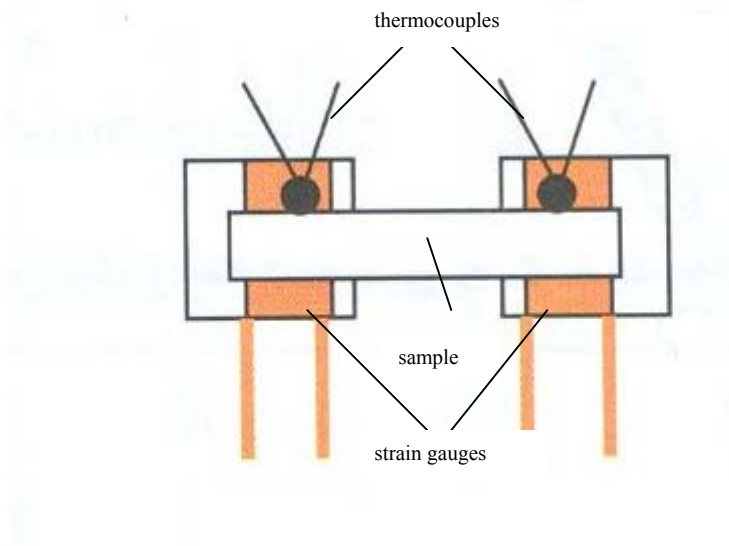


Fig. 13: Sample holder for Thermopower measurement

2.7 Simultaneous Measurement of Thermopower and Electrical Resistivity

The ULVAC ZEM 3 was used to measure Seebeck-coefficient and electrical resistivity of the samples in a temperature range of 20 to 300 °C. For the measurement of electrical resistivity a four-point technique is used and for Seebeck-effect a static dc method is used. Both, ρ and S , were measured in steps of 50 °C. During the measurement of thermopower temperature gradients of 10, 15 and 20 °C were applied in each step. The bar-shaped samples with a length of 7 to 9 mm and parallel surfaces at the bottom and the top were mounted in the sample holder and good contact between the lead and the sample was judged via performing a V-I-plot.

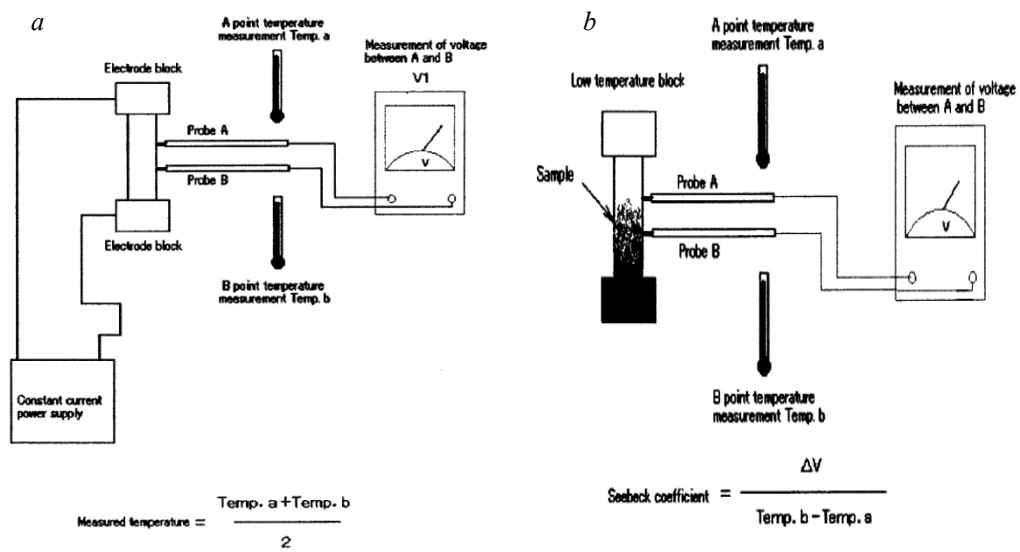


Fig. 14: Conceptual diagram for measurement of electrical resistance (a) and Seebeck coefficient (b) [33]

2.8 Measurement of Thermal Conductivity

A flashline 3000 (Anter Corporation) was used to measure the thermal conductivity in the temperature range of -50 to 300 °C. For temperatures higher than room temperature an equipment containing a furnace and a sample holder with space for five samples (4 samples + 1 reference) is available. For low temperatures another device, which can be cooled with liquid nitrogen, offers the opportunity for only one sample and one reference. With this device the thermal diffusivity α and the heat capacity C_p can be measured. The samples need to have a disc shape with a diameter of 6 mm. The surface of the discs is covered by graphite to guarantee an identical surface and therefore identical optical and thermal properties (immission and emission). A high-speed Xenon Pulse Source is used to illuminate the samples from one side and on the backside an infrared-detector measures the temperature change. Adjusting the charge voltage from 400 to 800 V can vary the power of the pulse. For my measurements a voltage of 600 V was used.

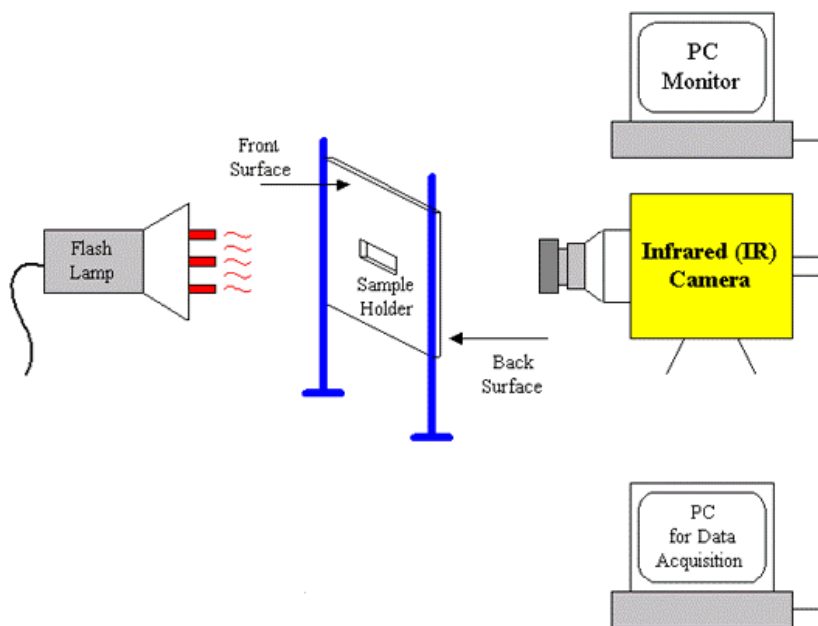


Fig. 15: Measurement principle of the flash line

The thermal conductivity can be derived from the data obtained by the measurement using the following formula:

$$(8) \quad \kappa = \rho \cdot \alpha \cdot C_p$$

The density ρ of the samples was measured at room temperature and extrapolated to the whole temperature range by using:

$$(9) \quad \rho = \frac{\rho_0}{(1 + 3 \cdot \alpha \cdot T)}$$

Here α is the thermal expansion coefficient, which was set to $1.358 \cdot 10^{-6} \text{ K}^{-1}$. ρ_0 is the density at room temperature and T the temperature.

For the determination of thermal diffusivity a general formula is used:

$$(10) \quad \alpha = \frac{c \cdot L^2}{t_{1/2}}$$

$t_{1/2}$ is the time at $T_{\max}/2$, which is measured. The formalism of Clark and Taylor, which considers heat losses, is used. L is the thickness of the sample and c a coefficient depending on the formalism used for calculating $t_{1/2}$.

In order to get the heat capacity of the sample a graphite reference with known heat capacity and the sample are illuminated with the same flash power and the unknown C_p of the sample can be derived from:

$$(11) \quad C_{p,S} = \frac{\rho_R \cdot L_R \cdot C_{p,R} \cdot \Delta T_R}{\rho_S \cdot L_S \cdot \Delta T_S}$$

$C_{p,S}$ and $C_{p,R}$ are the heat capacities of sample and reference, L_S and L_R are the thicknesses of sample and reference and ΔT the temperature differences before and after the light flash.

2.9 Measurement of the Shear Modulus

For the measurement of the shear modulus G the length of the bar-shaped samples has to exceed 15 mm. Thus the preparation of this sample was executed in two steps. First stoichiometric amounts of Cu-powder and P-powder (red phosphorus) were mixed with Sn-powder (-10 weight% of stoichiometric amount) and a hyperstoichiometric amount of SnI_4 . The total weight was about 10 g. The mixed powder was cold pressed and sealed under vacuum in a quartz tube. The furnace was heated up to 500 °C very slowly and the sample was kept at this temperature for 10 days before quenching it in cold water. In the second step the sample was ground and the obtained powder was transferred to a graphite die. The sample was hot pressed at 500 °C applying a pressure of 4 kN under argon atmosphere.

X-ray powder diffraction analysis was performed to check the formation of $\text{Sn}_{19.3}\text{Cu}_{4.7}\text{P}_{22}\text{I}_8$. The powder pattern showed a few weak additional peaks of unidentified phases. The density of the cylinder (diameter = 10 mm, height ~ 17 mm) was measured by using Archimedes' principle and was 4.884 g/cm³, corresponding to 87.5 % of the theoretical density. This value is somehow lower than the values of 90-95 % of theoretical density, which were achieved for samples synthesised using ball milling before hot pressing.

The cylindrical sample was cut into cuboids of 17 mm length for measuring the shear modulus G with a Malvern Gemini rheometer. The measurement was performed at a temperature range of -130 to 250 °C. For the low temperature measurement liquid nitrogen was used and a hot air stream for high temperatures heated the sample.



Fig. 16: Malvern Gemini rheometer

3. Results and Discussion

In this chapter the results of synthesis and structure refinement as well as the thermoelectric and elastic properties of the samples $\text{Sn}_{19.3}\text{Cu}_{4.7}\text{P}_{22}\text{I}_8$, $\text{Sn}_{18.3}\text{Cu}_{5.7}\text{P}_{22}\text{I}_8$, $\text{Sn}_{19.3}\text{Cu}_{4.7-x}\text{Zn}_x\text{P}_{22}\text{I}_8$ ($x = 1, 2, 3$), $\text{Sn}_{19.3}\text{Ag}_{1.7}\text{Zn}_3\text{P}_{22}\text{I}_8$ and $\text{Sn}_{19.3}\text{Au}_{1.7}\text{Zn}_3\text{P}_{22}\text{I}_8$ are presented and discussed.

3.1 Syntheses and Structures of Clathrate Compounds

3.1.1 Synthesis of $\text{Sn}_{19.3}\text{Cu}_{4.7}\text{P}_{22}\text{I}_8$ by a Standard Ampoule Procedure

In a first step the compound $\text{Sn}_{19.3}\text{Cu}_{4.7}\text{P}_{22}\text{I}_8$ was synthesised following the experimental procedure described in [15]. The reaction was carried out by a two-step annealing under vacuum. The following starting reagents were used: powders of tin, copper and red phosphorus and SnI_4 . They were mixed together in stoichiometric amounts with a total weight of 1 g. The mixed powder was pressed without lubricants (55 kg/cm^2) into a pellet, which was sealed in a glass tube under vacuum and placed in a furnace. The sample was heated up very slowly to a maximum temperature of 493°C within 12 days and then kept at this temperature for 2 days. It was cooled down to room temperature rapidly by quenching in H_2O . The pellet was reground and some powder was taken to perform X-ray Guinier diffraction powder analysis. The residual powder was again compacted under a pressure of 55 kg/cm^2 in a metal die and the obtained pellet was sealed under vacuum into a glass tube and placed in the furnace at 300°C . Within 5 days the temperature in the furnace was increased up to the maximum temperature of 508°C . Annealing at this temperature was done for 5 days. Then the sample was cooled switching-off the furnace. XRD was performed to verify sample composition.

Powder diffraction data revealed already formation of the inverse clathrate $\text{Sn}_{19.3}\text{Cu}_{4.7}\text{P}_{22}\text{I}_8$ after the first step of annealing. Besides the clathrate phase a small amount of the Sn-powder and some other unidentified peaks appeared in the pattern. No significant changes were observed after the second step of annealing. The crystal structure data as determined by Shatruck et al. [15] for the clathrate compound by a single-crystal X-ray diffraction experiment, were used as initial parameters in the Rietveld-refinement.

3.1.2 Synthesis of $\text{Sn}_{19.3}\text{Cu}_{4.7}\text{P}_{22}\text{I}_8$ by Ball Milling and Hot Pressing

There are two major disadvantages in using the method described in 3.1.1: (i) the long time duration until the compound has formed and (ii) the porous consistency of the clathrate material is not suitable for any thermoelectric investigations. In order to overcome these problems I tried to synthesise $\text{Sn}_{19.3}\text{Cu}_{4.7}\text{P}_{22}\text{I}_8$ using a combination of ball milling and hot pressing.

In the first step a stoichiometric mixture of the powders of the starting materials Cu, Sn, SnI_4 and red P was placed into a 45 ml steel crucible for the planetary mill “Pulverisette 4” (Fritsch). The total weight of the powder was 4.38 g. Before this procedure the crucible was filled with 93 g of steel balls with a diameter of 3 mm. To

avoid oxidation during the milling process the vials were filled up to $\frac{3}{4}$ with cyclohexane. The whole procedure was carried out stepwise, whereas the powder was checked by XRD after each step. In the following table the settings for the ball mill are shown:

Table 2: Single steps in the Ball Milling process

| | Weight of Balls [g] | Main Disk Speed | Ratio | Time [min] | Pause [min] | Repetitions |
|--------|---------------------|-----------------|-------|------------|-------------|-------------|
| step 1 | 92.88 | 170 | -2.5 | 10 | 5 | 11 |
| step 2 | 92.88 | 170 | -2.5 | 10 | 5 | 11 |
| step 3 | 92.88 | 250 | -2.5 | 10 | 5 | 11 |
| step 4 | 92.88 | 300 | -2.5 | 10 | 5 | 11 |

All these steps were done using the reverse mode, which means the direction of the main disk changes after each rotation period. The 4th column (RATIO) gives the ratio between the main disk rotation and the crucible holders' rotation.

X-ray-patterns showed that the predominant reflections were identified as Sn-reflections. Additionally some other unidentified weak reflections were detected, which could not be assigned to Bragg-positions of the starting materials. According to the grain size reduction caused by the milling line broadening of the peaks was observed. The increasing fraction of amorphous powder with milling time can be seen from the rise of the background radiation.

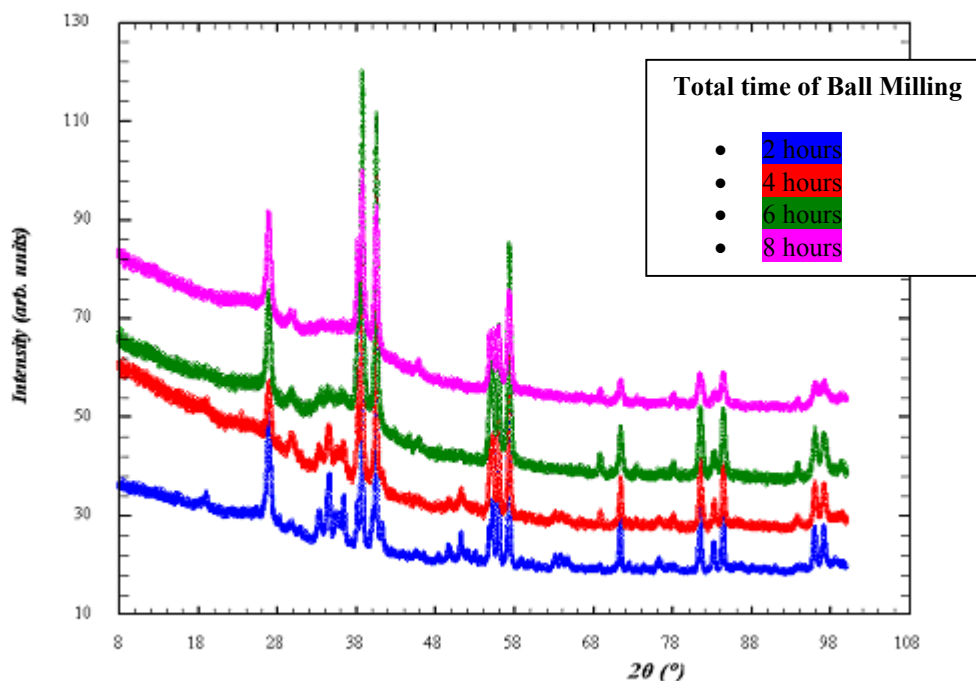


Fig. 17: Normalised intensities of the mechanical alloyed starting powders

After the 4th step the powder was pressed into a graphite die and transferred to the hot press. The sample was kept at a maximum temperature of 500 °C and a maximum pressure of 4 kN in argon atmosphere. A decrease of length of 2.5 mm as a function of reaction sintering/compaction was observed. After removing the sample from the graphite die the adhesive carbon was removed by grinding. The shape of the sample appeared to be a cylindrical pill with a diameter of 1 cm and a length of 4.5 cm. A small piece was cut off by a diamond saw and powdered for X-ray diffraction. The structure of the inverse clathrate $\text{Sn}_{19.3}\text{Cu}_{4.7}\text{P}_{22}\text{I}_8$ was observed in the diffractogram and additionally peaks of the Sn-powder and some small peaks of unidentified phases. The Sn-peaks were significantly higher than the Sn-reflections of the sample synthesised by the ampoule technique. As initial structural model for the Rietveld-refinement the data of the sample synthesised with method 3.1.1 were used. Sn was refined as a second phase using the data of the Rietveld-refinement of pure Sn-powder (Fig. 18).

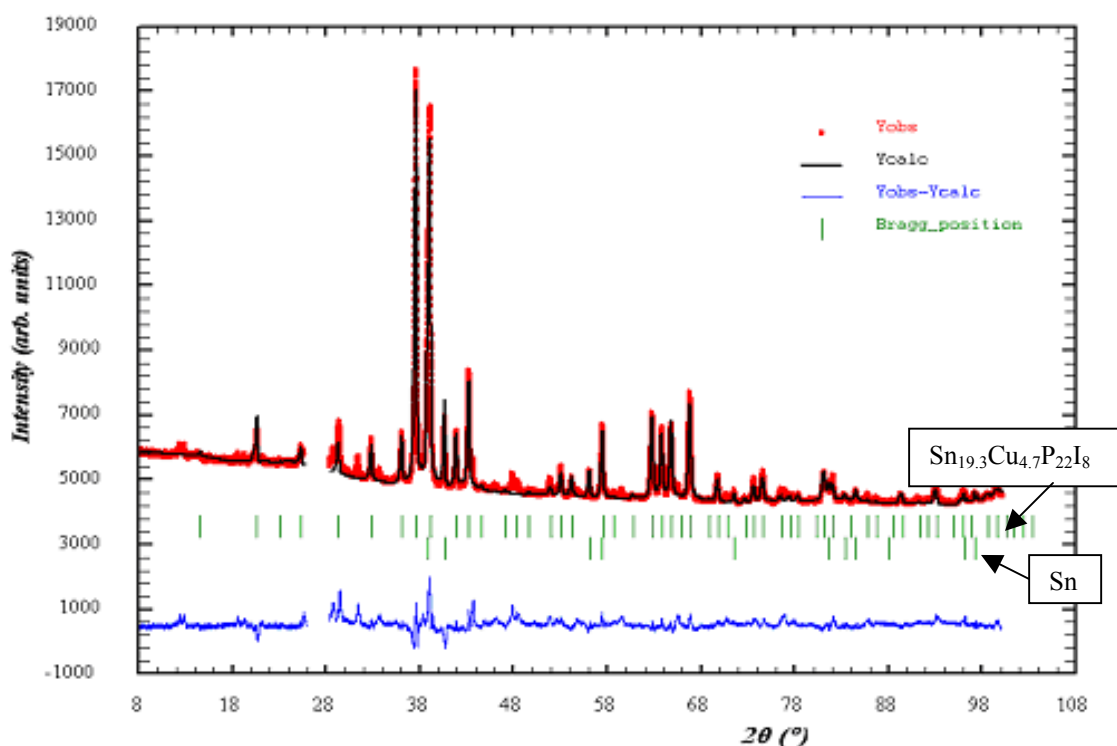


Fig. 18: First sample synthesised with Ball Mill and Hot Press

In order to get a single-phase product in the first step the amount of Sn was reduced by 10 weight%. Additionally, the total weight of the samples was increased to 7 g in order to get a cylinder with a height of 10 mm as a final product out of the hot press. The XRD-analysis showed a significant reduction, but the most prominent peak of Sn ((101)-reflection) was still in evidence. Thus in the next steps the amounts of SnI_4 and P were increased, while the already reduced amount of Sn was kept constant at a level of -10 weight%. The two samples obtained from the new composition didn't show any residual tin. Moreover the intensities in the powder pattern of the unidentified

phases were nearly gone. Only one unidentified peak in-between the two clathrate-peaks of highest intensity didn't change at all, this peak was also present in the diffractogram of the sample synthesised by the standard ampoule technique. Further increasing of the initial weight of P or SnI_4 (each 5 weight%) didn't show any significant changes in the XRD-patterns. The changes in main disk speed and total duration of ball milling could not produce any distinguishable results. Hot pressing seems to be the necessary and decisive step for formation of the clathrate-I-structure. The density of the samples was measured using Archimedes' principle. In most samples it reached a value of 94 % of the density calculated from the X-ray data (5.576 g/cm^3).

In the following graph the reduction in intensity of the Sn-peak is shown until its complete disappearance for the samples with an increased amount of SnI_4 in the starting composition:

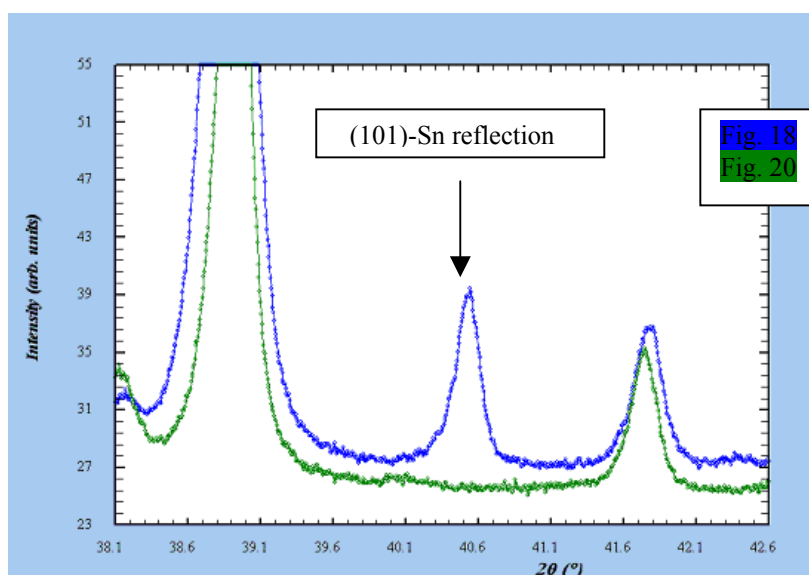


Fig. 19: Change of Sn-contamination in $\text{Sn}_{19.3}\text{Cu}_{4.7}\text{P}_{22}\text{I}_8$

The whole diffraction pattern of the sample, whereof the thermoelectric measurements have been performed, is shown below. Only at 38° in 2θ appears a significant unidentified additional peak.

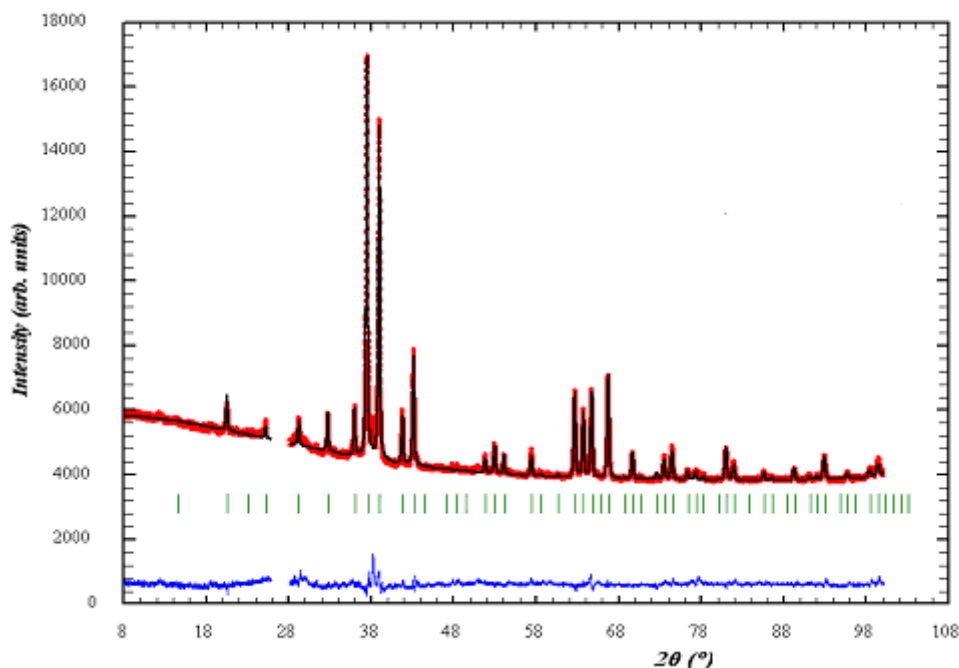


Fig. 20: $\text{Sn}_{19.3}\text{Cu}_{4.7}\text{P}_{22}\text{I}_8$ synthesised using Ball Mill and Hot Press

With the combination of ball milling followed by hot pressing it is possible to synthesise the inverse clathrate within one day and moreover the final shape and density are suitable to cut out bar- and disc-shaped pieces for the investigation of thermoelectric properties.

3.1.3 Synthesis and Structure of new Clathrate-I-Compounds: $\text{Sn}_{18.3}\text{Cu}_{5.7}\text{P}_{22}\text{I}_8$, $\text{Sn}_{19.3}\text{Cu}_{4.7-x}\text{Zn}_x\text{P}_{22}\text{I}_8$ ($x = 1, 2, 3$), $\text{Sn}_{19.3}\text{Ag}_{1.7}\text{Zn}_3\text{P}_{22}\text{I}_8$ and $\text{Sn}_{19.3}\text{Au}_{1.7}\text{Zn}_3\text{P}_{22}\text{I}_8$

All these samples were prepared and synthesised following the optimised procedure outlined above. Stoichiometric amounts of the starting powders Sn, P, SnI_4 , Cu and Zn, modified using the results received from $\text{Sn}_{19.3}\text{Cu}_{4.7}\text{P}_{22}\text{I}_8$ were weighed and inserted into the ball mill crucibles. Cyclohexane was used during the milling to avoid oxidation. Afterwards the powder was transferred into a graphite die and hot pressed at 500 °C at 4 kN in Ar-atmosphere. The detailed conditions for ball milling are given in the table below:

Table 3: Ball Mill conditions

| Weight of balls [g] | Main Disk Speed | Ratio | Time [min] | Pause [min] | repetitions |
|---------------------|-----------------|-------|------------|-------------|-------------|
| 92.88 | 250 | -2.5 | 10 | 6 | 15 |

The densities of the resulting cylindrical shaped samples were measured using Archimedes' principle. The values reached at least 92 % of the theoretical density. To investigate the effect of incorporating Ag and Au, two completely new elements in a framework of an inverse clathrate, two samples with the nominal composition

$\text{Sn}_{19.3}\text{Ag}_{1.7}\text{Zn}_3\text{P}_{22}\text{I}_8$ and $\text{Sn}_{19.3}\text{Au}_{1.7}\text{Zn}_3\text{P}_{22}\text{I}_8$ were prepared. The density for those compounds didn't reach values as high as all the other samples. The reason for this could be an insufficient compaction during the hot press process. The formation of the clathrate-I-structure was confirmed and analysed in detail via Rietveld-refinement.

The crystal structure data published in [15] were standardised using the program Structure Tidy before using them as a starting point in Rietveld-refinement and the result is consistent with the data found in [20]. For transformation an origin shift of (0.5 0.5 0.5) is necessary. The standardised atomic positions are listed in the following table:

Table 4: Standardised data of the clathrate-I-type (space group: $\text{Pm}\bar{3}\text{n}$) $\text{Sn}_{19.3}\text{Cu}_{4.7}\text{P}_{22}\text{I}_8$

| Atom | x/a | y/b | z/c | site |
|------|---------|---------|---------|------|
| I(2) | 0 | 0 | 0 | 2a |
| I(1) | 0.25 | 0 | 0.5 | 6c |
| P(2) | 0.25 | 0.5 | 0 | 6d |
| P(1) | 0.19180 | 0.19180 | 0.19180 | 16i |
| M(1) | 0 | 0.13410 | 0.30680 | 24k |
| M(2) | 0 | 0.07400 | 0.32080 | 24k |

The results of the structure refinements of all samples are presented in the following tables:

Table 5: Structural data (clathrate type-I, space group: $Pm\bar{3}n$, $Z = 1$; Guinier, Fe $K_{\alpha 1}$) for $Sn_{19.3}Cu_{4.7-x}Zn_xP_{22}I_8$ ($x = 1, 2, 3$)

| Parameter/Compound | $Sn_{19.3}Cu_{3.7}Zn_1P_{22}I_8$ | $Sn_{19.3}Cu_{2.7}Zn_2P_{22}I_8$ | $Sn_{19.3}Cu_{1.7}Zn_3P_{22}I_8$ |
|---|---|---|---|
| Synthesis | Ball Mill + Hot Press | Ball Mill + Hot Press | Ball Mill + Hot Press |
| Composition from refinement | $Sn_{19.3}Cu_{3.7}Zn_1P_{21.2}\square_{0.8}I_8$ | $Sn_{19.3}Cu_{2.7}Zn_2P_{20.9}\square_{1.1}I_8$ | $Sn_{19.3}Cu_{1.7}Zn_3P_{19.9}\square_{2.1}I_8$ |
| 2θ range (degrees) | $8 \leq 2\theta \leq 100$ | $8 \leq 2\theta \leq 100$ | $8 \leq 2\theta \leq 100$ |
| a [nm] | 1.08773(4) | 1.08876(3) | 1.08915(3) |
| V [nm ³] | 1.2869(2) | 1.2906(1) | 1.29201(9) |
| ρ_{calc} [g/cm ³] | 5.550 | 5.540 | 5.536 |
| ρ_{obs} [g/cm ³] | 5.199 | 5.067 | 5.037 |
| Reflections in refinement | 80 | 80 | 81 |
| $R_F = \Sigma F_o - F_c / \Sigma F_o$ | 0.111 | 0.097 | 0.076 |
| $R_I = \Sigma I_o - I_c / \Sigma I_o$ | 0.097 | 0.079 | 0.073 |
| χ^2 | 0.410 | 0.601 | 0.6530 |
| Atom parameters | | | |
| I in 2a (0, 0, 0) | | | |
| $B_{eq} (B_{iso}) 10^2 (nm^2)$ | 0.113 | 0.228 | 0.574 |
| Occ. | 1 | 1 | 1 |
| I in 6c ($\frac{1}{4}, 0, \frac{1}{2}$) | | | |
| $B_{eq} (B_{iso}) 10^2 (nm^2)$ | 0.572 | 0.529 | 0.295 |
| Occ. | 1 | 1 | 1 |
| P in 6d ($\frac{1}{4}, \frac{1}{2}, 0$) | | | |
| $B_{eq} (B_{iso}) 10^2 (nm^2)$ | 0.717 | 0.812 | 0.886 |
| Occ. | 0.86(4) P + 0.14 \square | 0.81(5) P + 0.19 \square | 0.65(5) P + 0.35 \square |
| P in 16i (x, x, x), x | 0.18910(21) | 0.18969(17) | 0.19191(15) |
| $B_{eq} (B_{iso}) 10^2 (nm^2)$ | 0.935 | 0.830 | 0.458 |
| Occ. | 1 | 1 | 1 |
| Sn1 in 24k (0, y, z), y, z | y: 0.13715(10) z: 0.31666(17) | y: 0.13763(9) z: 0.31656(15) | y: 0.13733(9) z: 0.31913(13) |
| $B_{eq} (B_{iso}) 10^2 (nm^2)$ | 0.121 | 0.526 | 0.946 |
| Occ. | 0.62(6) | 0.62(2) | 0.61(1) |
| Sn2 in 24k (0, y, z), y, z | y: 0.08923(45) z: 0.30652(44) | y: 0.09264(35) z: 0.30690(38) | y: 0.09734(31) z: 0.30497(32) |
| $B_{eq} (B_{iso}) 10^2 (nm^2)$ | 0.973 | 0.454 | 0.780 |
| Occ. | 0.18(5) | 0.18(2) | 0.19(4) |
| Cu1 in 24k (0, y, z), y, z | y: 0.13715(10) z: 0.31666(17) | y: 0.13763(9) z: 0.31656(15) | y: 0.13733(9) z: 0.31913(13) |
| $B_{eq} (B_{iso}) 10^2 (nm^2)$ | 0.121 | 0.526 | 0.946 |
| Occ. | 0.06(-) | 0.05(6) | 0.03(3) |
| Cu2 in 24k (0, y, z), y, z | y: 0.08923(45) z: 0.30652(44) | y: 0.09264(35) z: 0.30690(38) | y: 0.09734(31) z: 0.30497(32) |
| $B_{eq} (B_{iso}) 10^2 (nm^2)$ | 0.973 | 0.454 | 0.780 |
| Occ. | 0.06(-) | 0.05(6) | 0.04(1) |
| Zn1 in 24k (0, y, z), y, z | y: 0.13715(10) z: 0.31666(17) | y: 0.13763(9) z: 0.31656(15) | y: 0.13733(9) z: 0.31913(13) |
| $B_{eq} (B_{iso}) 10^2 (nm^2)$ | 0.121 | 0.526 | 0.946 |
| Occ. | 0.02(-) | 0.04(2) | 0.05(4) |
| Zn2 in 24k (0, y, z), y, z | y: 0.08923(45) z: 0.30652(44) | y: 0.09264(35) z: 0.30690(38) | y: 0.09734(31) z: 0.30497(32) |
| $B_{eq} (B_{iso}) 10^2 (nm^2)$ | 0.973 | 0.454 | 0.780 |
| Occ. | 0.02(-) | 0.04(2) | 0.07(1) |

Table 6: Structural data (clathrate type-I, space group: $Pm\bar{3}n$, $Z=1$; Guinier, Fe $K_{\alpha 1}$) for $Sn_{19.3}Cu_{4.7}P_{22}I_8$, $Sn_{19.3}Ag_{1.7}Zn_3P_{22}I_8$, $Sn_{19.3}Au_{1.7}Zn_3P_{22}I_8$ and $Sn_{18.3}Cu_{5.7}P_{22}I_8$

| Parameter/Compound | $Sn_{19.3}Cu_{4.7}P_{22}I_8$ | $Sn_{18.3}Cu_{5.7}P_{22}I_8$ | $Sn_{19.3}Ag_{1.7}Zn_3P_{22}I_8$ | $Sn_{19.3}Au_{1.7}Zn_3P_{22}I_8$ |
|---|----------------------------------|----------------------------------|---|---|
| Synthesis | Ball Mill + Hot Press | Ball Mill + Hot Press | Ball Mill + Hot Press | Ball Mill + Hot Press |
| Composition from refinement (at%) | $Sn_{19.3}Cu_{4.7}P_{22}I_8$ | $Sn_{18.3}Cu_{5.7}P_{22}I_8$ | $Sn_{19.3}Ag_{1.7}Zn_3P_{19.2}\square_{2.8}I_8$ | $Sn_{19.3}Au_{1.7}Zn_3P_{18.8}\square_{3.2}I_8$ |
| 2 θ range (degrees) | $8 \leq 2\theta \leq 100$ | $8 \leq 2\theta \leq 100$ | $8 \leq 2\theta \leq 100$ | $8 \leq 2\theta \leq 100$ |
| a [nm] | 1.08683(5) | 1.08640(2) | 1.09376(3) | 1.09429(4) |
| V [nm ³]: | 1.2837(2) | 1.2822(2) | 1.3084(2) | 1.3104(2) |
| ρ_{calc} [g/cm ³] | 5.576 | 5.497 | 5.563 | 5.747 |
| ρ_{obs} [g/cm ³] | 5.238 | 5.180 | 4.720 | 4.960 |
| Reflections in refinement | 80 | 80 | 81 | 81 |
| $R_F = \Sigma F_o - F_c / \Sigma F_o$ | 0.113 | 0.161 | 0.117 | 0.186 |
| $R_I = \Sigma I_o - I_c / \Sigma I_o$ | 0.120 | 0.148 | 0.092 | 0.235 |
| χ^2 | 1.45 | 0.794 | 2.06 | 7.22 |
| I in 2a (0, 0, 0) | | | | |
| B_{eq} (B_{iso}) 10 ² (nm ²) | 0.156 | 0.5(-) | 0.525 | 0.5(-) |
| Occ. | 1 | 1 | 1 | 1 |
| I in 6c (1/4, 0, 1/2) | | | | |
| B_{eq} (B_{iso}) 10 ² (nm ²) | 0.814 | 0.5(-) | 0.238 | 0.5(-) |
| Occ. | 1 | 1 | 1 | 1 |
| P in 6d (1/4, 1/2, 0) | | | | |
| B_{eq} (B_{iso}) 10 ² (nm ²) | 0.874 | 0.5(-) | 0.978 | 0.5(-) |
| Occ. | 1 | 1 | 0.54(3) P + 0.46 \square | 0.46(3) P + 0.54 \square |
| P in 16i (x, x, x), x | 0.18785(24) | 0.18886(26) | 0.19313(25) | 0.19594(47) |
| B_{eq} (B_{iso}) 10 ² (nm ²) | 0.964 | 0.5(-) | 0.858 | 0.5(-) |
| Occ. | 1 | 1 | 1 | 1 |
| Sn1 in 24k (0, y, z), y, z | y: 0.13382(9) z: 0.31409(16) | y: 0.13270(10) z: 0.31360(17) | y: 0.14124(16) z: 0.32905(19) | y: 0.14241(28) z: 0.33614(32) |
| B_{eq} (B_{iso}) 10 ² (nm ²) | 0.732 | 0.5(-) | 0.353 | 0.5(-) |
| Occ. | 0.71(2) | 0.69(2) | 0.57(2) | 0.57(2) |
| Sn2 in 24k (0, y, z), y, z | y: 0.07639(66) z: 0.31079(75) | y: 0.07255(75) z: 0.30976(86) | y: 0.10347(39) z: 0.29870(33) | y: 0.10174(66) z: 0.29685(54) |
| B_{eq} (B_{iso}) 10 ² (nm ²) | 0.394 | 0.5(-) | 0.377 | 0.5(-) |
| Occ. | 0.09(2) | 0.07(1) | 0.24(1) | 0.23(2) |
| Cu/Ag/Au1 in 24k (0, y, z), y, z | y: 0.13382(9) z: 0.31409(16) | y: 0.13270(10) z: 0.31360(17) | y: 0.14124(16) z: 0.32905(19) | y: 0.14241(28) z: 0.33614(32) |
| B_{eq} (B_{iso}) 10 ² (nm ²) | 0.732 | 0.5(-) | 0.353 | 0.5(-) |
| Occ. | 0.10(1) | 0.12(-) | 0.02(1) | 0.02(1) |
| Cu/Ag/Au2 in 24k (0, y, z), y, z | y: 0.07639(66) z: 0.31079(75) | y: 0.07255(75) z: 0.30976(86) | y: 0.10347(39) z: 0.29870(33) | y: 0.10174(66) z: 0.29685(54) |
| B_{eq} (B_{iso}) 10 ² (nm ²) | 0.394 | 0.5(-) | 0.377 | 0.5(-) |
| Occ. | 0.10(2) | 0.12(-) | 0.05(1) | 0.050 |
| Zn1 in 24k (0, y, z), y, z | --- | --- | y: 0.14124(16) z: 0.32905(19) | y: 0.14241(28) z: 0.33614(32) |
| B_{eq} (B_{iso}) 10 ² (nm ²) | --- | --- | 0.353 | 0.5(-) |
| Occ. | --- | --- | 0.05(4) | 0.05(3) |
| Zn2 in 24k (0, y, z), y, z | --- | --- | y: 0.10347(39) z: 0.29870(33) | y: 0.10174(66) z: 0.29685(54) |
| B_{eq} (B_{iso}) 10 ² (nm ²) | --- | --- | 0.377 | 0.5(-) |
| Occ. | --- | --- | 0.08(2) | 0.08(1) |

The patterns for the compounds $\text{Sn}_{18.3}\text{Cu}_{5.7}\text{P}_{22}\text{I}_8$ and $\text{Sn}_{19.3}\text{Au}_{1.7}\text{Zn}_3\text{P}_{22}\text{I}_8$ showed the clathrate-I-structure as a predominant phase, but many peaks with an intensity of 1 – 10 % of the (320)-reflection of the clathrate indicate the existence of secondary phases. Thus the refinement of both compounds was done without refining the isotropic temperature factors. Due to the complex situation in a quinary system the attempt to identify the additional phases failed, because up to now even in the ternary system Cu-P-Sn only parts of the copper-rich region are investigated [21]. In most cases because of the negligible effect the distribution onto the two split positions in the 24k-site was not performed for Cu and Zn. In the samples with the nominal composition $\text{Sn}_{19.3}\text{Cu}_{4.7-x}\text{Zn}_x\text{P}_{22}\text{I}_8$ the substitution of Cu by Zn could not be investigated because of the very small effect on X-rays (only one electron difference and thus almost no difference in the atomic form factor).

With increasing Zn-content the additional peak at 38° in 2θ is decreasing until it completely disappears for the sample $\text{Sn}_{19.3}\text{Cu}_{1.7}\text{Zn}_3\text{P}_{22}\text{I}_8$, which shows a practically single-phase powder pattern (Fig. 21).

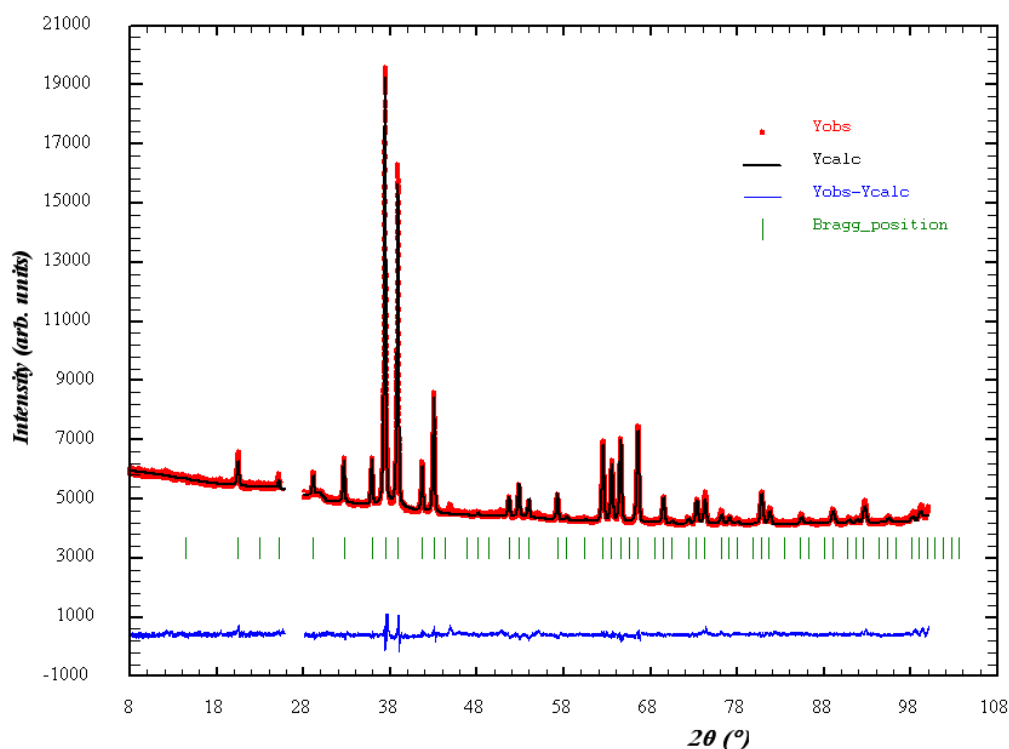


Fig. 21: Refined powder pattern of $\text{Sn}_{19.3}\text{Cu}_{1.7}\text{Zn}_3\text{P}_{22}\text{I}_8$

Atom substitution of Cu by Zn, Ag and Au or Sn by Cu in case of $\text{Sn}_{18.3}\text{Cu}_{5.7}\text{P}_{22}\text{I}_8$ should lead to a change in the lattice parameters. Thus they were determined using Ge ($a = 0.5657906$ nm) as an internal standard on the Guinier-Diffractometer with $\text{FeK}_{\alpha 1}$ -radiation ($\lambda = 0.193604$ nm). Although the lattice parameters of $\text{Sn}_{19.3}\text{Cu}_{4.7}\text{P}_{22}\text{I}_8$ and $\text{Sn}_{18.3}\text{Cu}_{5.7}\text{P}_{22}\text{I}_8$ are slightly different (Table 4), which would indicate a solid solubility region, it stays unclear, if the compound $\text{Sn}_{18.3}\text{Cu}_{5.7}\text{P}_{22}\text{I}_8$, which deviates from the Zintl formalism, is formed. When Cu is substituted by Zn, the lattice

parameter shows a significant increase (Fig. 22). Up to the nominal composition $\text{Sn}_{19,3}\text{Cu}_{2,7}\text{Zn}_2\text{P}_{22}\text{I}_8$ the change of lattice parameters shows an almost linear behaviour, only the sample $\text{Sn}_{19,3}\text{Cu}_{1,7}\text{Zn}_3\text{P}_{22}\text{I}_8$ deviates slightly (Fig. 22). The reason might be, that for this composition the Zn-content does not reach the nominal amount. This result is affirmed as well by the powder pattern, where a small peak at 55.1° in 2θ indicates the existence of a small amount of non-reacted Zn. This peak can be assigned to the (101)-reflection of zinc and could not be found in the patterns of the other Zn-containing samples. The successful substitution of Cu by Ag and Au can be clearly seen from the significant increase of the lattice parameter a . The small difference in the atomic radii of Ag (144.5 pm) and Au (144.2 pm) compared to the rather large difference compared to Cu (127.8 pm), can explain the very similar values for a .

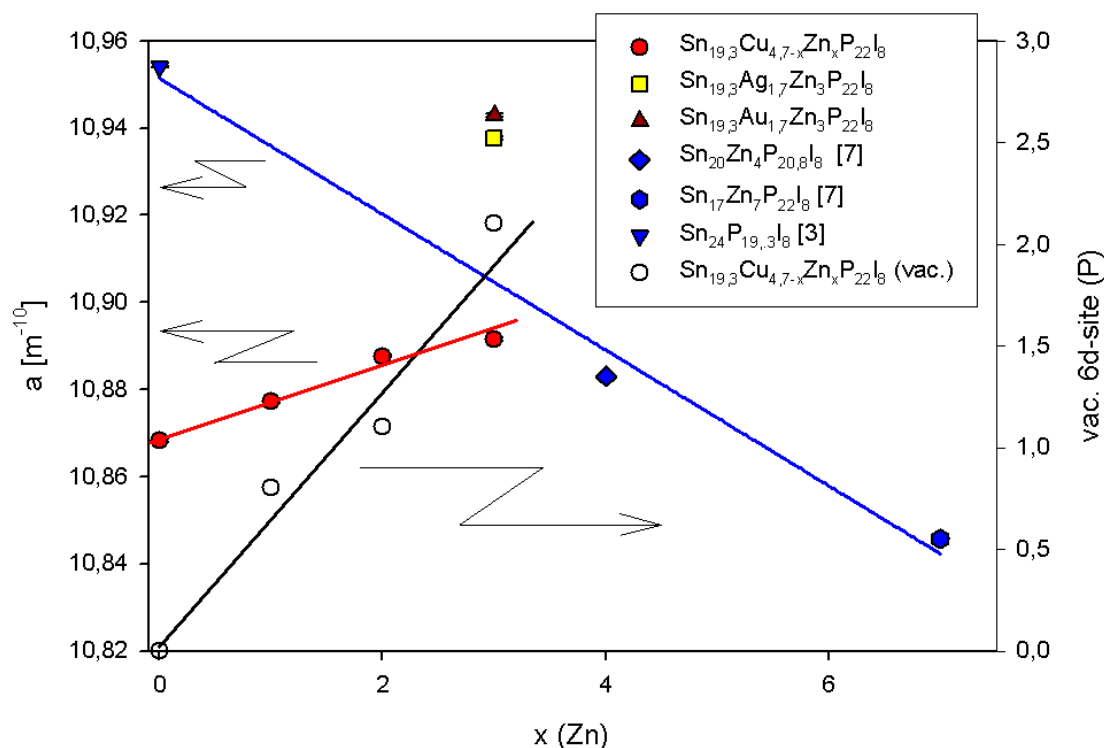


Fig. 22: Change of the lattice parameter a in the samples $\text{Sn}_{19,3}\text{Cu}_{4,7-x}\text{Zn}_x\text{P}_{22}\text{I}_8$ ($x = 1, 2, 3$) by substitution of Cu by Zn (almost linear (red line)) and in $\text{Sn}_{19,3}\text{Cu}_{1,7}\text{Zn}_3\text{P}_{22}\text{I}_8$ by Ag and Au in the Cu-position; the lattice parameters of $\text{Sn}_{24}\text{P}_{19,3}\text{I}_8$, $\text{Sn}_{20}\text{Zn}_4\text{P}_{20,8}\text{I}_8$ and $\text{Sn}_{17}\text{Zn}_7\text{P}_{22}\text{I}_8$ are plotted in blue; the dependency of vacancy formation on the Zn-content is shown with open circles (black line)

From Rietveld-refinement the Zn-containing samples form vacancies in the 6d-position of phosphorus depending on the amount of substitution of Cu by Zn. In this case these vacancies are somehow overcompensating the additional electrons coming from the Zn. This effect seems to be amplified by the substitution of Cu by Ag and Au.

3.2. Thermoelectric Performance

As already mentioned in the introduction the efficiency of thermoelectric materials is characterised by the dimensionless figure of merit ZT . The thermoelectric power factor (S^2/ρ) maximizes somewhere between metals and semiconductors (Fig. 23). Good thermoelectric materials are typically heavily doped semiconductors or semimetals with carrier concentrations of 10^{19} to 10^{21} carriers/cm³. There should only be a single type of charge carriers, because mixed n-type and p-type conduction leads to opposing Seebeck effect and low thermopower. Thus good thermoelectric materials should possess band gaps large enough to have only single charge carrier type but small enough to sufficiently high doping and high mobility, which leads to high electrical conductivity.

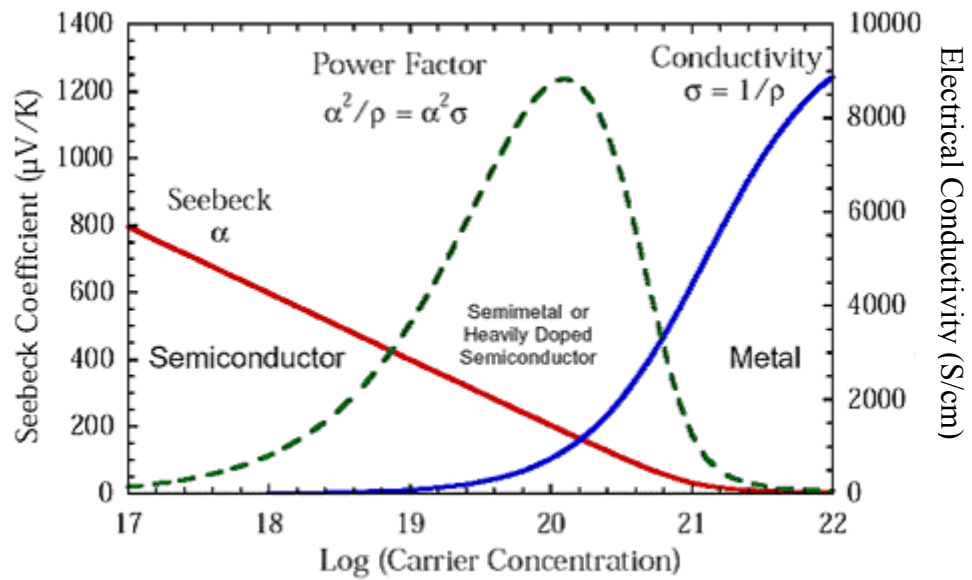


Fig. 23: Development of the thermoelectric power factor dependent on the charge carriers

3. 2. 1 Substitutions in the Clathrate Framework

In the first step the electrical resistivity of the compound $\text{Sn}_{19.3}\text{Cu}_{4.7}\text{P}_{22}\text{I}_8$ was measured to get a first indication for its thermoelectric value. In principle clathrate compounds belonging to Zintl phases should exhibit semiconducting properties. The value of $4.3 \text{ } \Omega\text{m}$ at 300 K showed, that the electrical resistivity has to be reduced to expand into the interesting region for thermoelectric applications. To increase the electrical conductivity two different routes were chosen. One attempt was to substitute one of the Sn-atoms by a Cu-atom, which would lead to the composition $\text{Sn}_{18.3}\text{Cu}_{5.7}\text{P}_{22}\text{I}_8$. By this substitution the total number of electrons in the clathrate is reduced by 3 electrons per formula unit and thus an increase in electrical conductivity by p-doping is expected. To get an n-type semiconductor I tried to substitute the Cu-atoms in the framework by Zn. With every Zn-atom an additional electron enters the framework. Therefore in total a series of three samples with the chemical compositions $\text{Sn}_{19.3}\text{Cu}_{4.7-x}\text{Zn}_x\text{P}_{22}\text{I}_8$ ($x = 1, 2, 3$) were synthesised. To get a first idea of the effect of Ag and Au as new transition metals in the framework of the inverse clathrate-I-compounds, the compound $\text{Sn}_{19.3}\text{Cu}_{1.7}\text{Zn}_3\text{P}_{22}\text{I}_8$, which shows the lowest resistivity at room temperature, was chosen to perform substitution of Cu by silver and gold.

3.2.2 Electrical Resistivity

The electrical resistivity of all samples was measured using the devices described in 2.5 or 2.7. In the case of $\text{Sn}_{18.3}\text{Cu}_{5.7}\text{P}_{22}\text{I}_8$, where a p-doping of the Zintl-phase $\text{Sn}_{19.3}\text{Cu}_{4.7}\text{P}_{22}\text{I}_8$ was expected, the electrical resistivity did not show a decrease. A possible explanation for the increased electrical resistivity could be, that instead of the formation of the expected compound some additional phases with lower electrical conductivity have formed. In contrast to this result for the Zn-containing clathrates a decrease of the resistivity with increasing zinc-content was indeed observed.

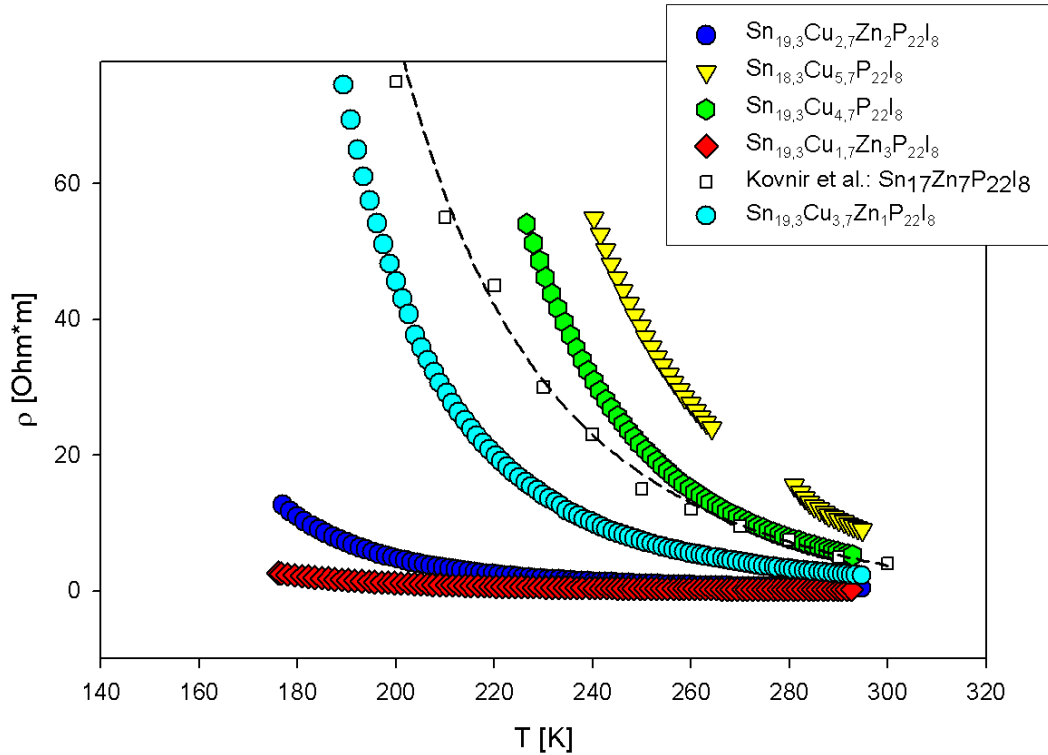


Fig. 24: Electrical resistivity for $\text{Sn}_{18.3}\text{Cu}_{5.7}\text{P}_{22}\text{I}_8$, $\text{Sn}_{19.3}\text{Cu}_{4.7}\text{P}_{22}\text{I}_8$ and for $\text{Sn}_{19.3}\text{Cu}_{4.7-x}\text{Zn}_x\text{P}_{22}\text{I}_8$ ($x = 1, 2, 3$) measured at low temperatures (colored symbols) as compared to the values published in [7] (open squares; dashed line is an exponential regression using formula (12))

In Fig. 24 the values of all the samples are compared to the values of $\text{Sn}_{17}\text{Zn}_7\text{P}_{22}\text{I}_8$ [7], which is consistent with the Zintl concept. The data points for $\text{Sn}_{18.3}\text{Cu}_{5.7}\text{P}_{22}\text{I}_8$ in-between 260-280 K dropped out because of a measurement equipment problem. The exponential increase of electrical resistivity is typical for semiconductors. For the thermally activated conductivity of semiconductors the slope of the temperature dependence can be described with the following formula:

$$(12) \quad \rho(T) = \rho_0 + C \cdot \exp \frac{\Delta E_{\text{gap}}}{2 \cdot k_B \cdot T}$$

Here $\rho(T)$ is the electrical resistivity at temperature T , ρ_0 is the resistivity at infinitely high temperature, ΔE_{gap} is the band gap and k_B is the Boltzmann-constant. With the program Table Curve (Systat Software GmbH) the parameters ρ_0 , C and ΔE_{gap} were fitted to the data points obtained by the measurement. For the samples $\text{Sn}_{18.3}\text{Cu}_{5.7}\text{P}_{22}\text{I}_8$ and $\text{Sn}_{19.3}\text{Cu}_{4.7}\text{P}_{22}\text{I}_8$ the slope of the measured curve could not be fitted unless allowing physically meaningless negative values for ρ_0 . In case of the Zn-containing samples the fitting was successful with r^2 -values better then 0.999.

The band gaps in eV were calculated using the result for the fitted parameter ΔE_{gap} and $k_B = 8.617343 \cdot 10^{-5}$ eV/K and presented in the following table:

Table 7: Band gaps (ΔE_{gap}) of the Zn-containing samples

| Compound | $\text{Sn}_{19.3}\text{Cu}_{3.7}\text{Zn}_1\text{P}_{22}\text{I}_8$ | $\text{Sn}_{19.3}\text{Cu}_{2.7}\text{Zn}_2\text{P}_{22}\text{I}_8$ | $\text{Sn}_{19.3}\text{Cu}_{1.7}\text{Zn}_3\text{P}_{22}\text{I}_8$ |
|---------------|---|---|---|
| Band gap [eV] | 0.29 | 0.26 | 0.21 |

These values fit quite well to the value of 0.25 eV for $\text{Sn}_{17}\text{Zn}_7\text{P}_{22}\text{I}_8$ given in [7].

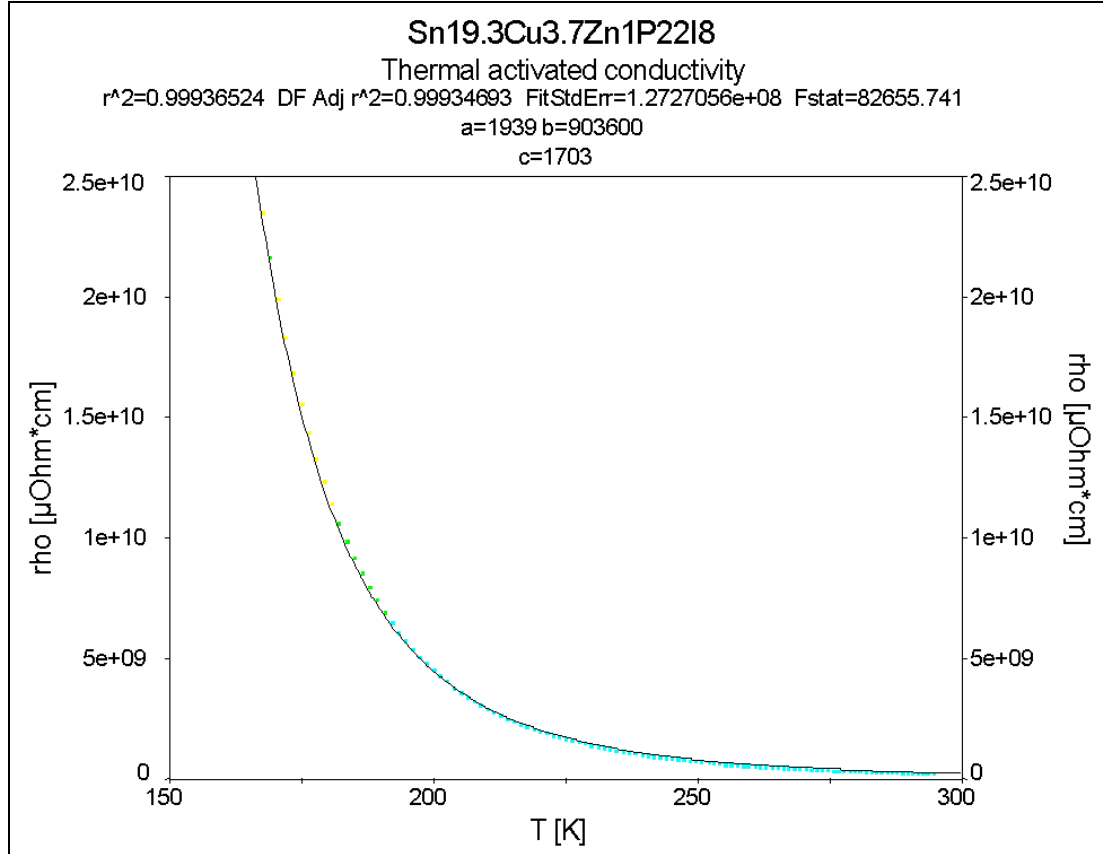


Fig. 25: Result of the fitting for the compound $\text{Sn}_{19.3}\text{Cu}_{3.7}\text{Zn}_1\text{P}_{22}\text{I}_8$: The parameters a , b and c are the fitted parameters and are related to equation (12) by:

$$\rho(T) = \rho_0 (= a) + C (= b) \cdot \exp\left(\frac{\Delta E_{gap}}{2 \cdot k_B} (= c) \cdot \frac{1}{T}\right)$$

The colors of the measured points show, how good they fit to the calculated curve (black line): starting from red (bad)-yellow-green-blue (good)

The electrical resistivity data obtained for the samples $\text{Sn}_{18.3}\text{Cu}_{5.7}\text{P}_{22}\text{I}_8$ and $\text{Sn}_{19.3}\text{Cu}_{4.7}\text{P}_{22}\text{I}_8$ show a temperature dependency, which usually can be observed, when some kind of hopping behaviour dominates the electrical conduction. This characteristic temperature dependency was first described by Mott [19] for amorphous silicon and is typical for conductivity of localised electrons. In this case the electron movement relies on tunneling processes, which means, the electrons are tunneling from one localised level to an adjacent level. This phenomenon is often denoted as hopping conduction. A precondition for this hopping mechanism is the overlap of the wave functions of an occupied and an unoccupied state. The temperature dependency of the electrical conductivity can be described in the following context:

$$(13) \quad \sigma = \sigma_0 \cdot \exp\left(-\left(\frac{T_0}{T}\right)^{1/4}\right)$$

where T_0 is:

$$(14) \quad T_0 = \frac{(4 \cdot \alpha)^3}{9 \cdot \pi \cdot D(E_F) \cdot k_B}$$

Here α is a parameter for the decay of the wave function, $D(E_F)$ the density of states at the Fermi-level and k_B the Boltzmann-constant.

Sometimes an exponent $1/2$ fits better to experimental data, when the density of states in the region of the Fermi-level is not constant but increasing with higher energy.

When I tried to fit the observed data for the two samples to this hopping conduction theory using the program Table Curve the agreement for both exponents was rather good. For the samples $\text{Sn}_{18.3}\text{Cu}_{5.7}\text{P}_{22}\text{I}_8$ and $\text{Sn}_{19.3}\text{Cu}_{4.7}\text{P}_{22}\text{I}_8$ no significant differences appear when the exponent in equation (13) is changed to $1/2$. The Zn-containing samples show a better agreement, when the exponent $1/2$ is applied to the measurement data (Fig. 26 + 27).

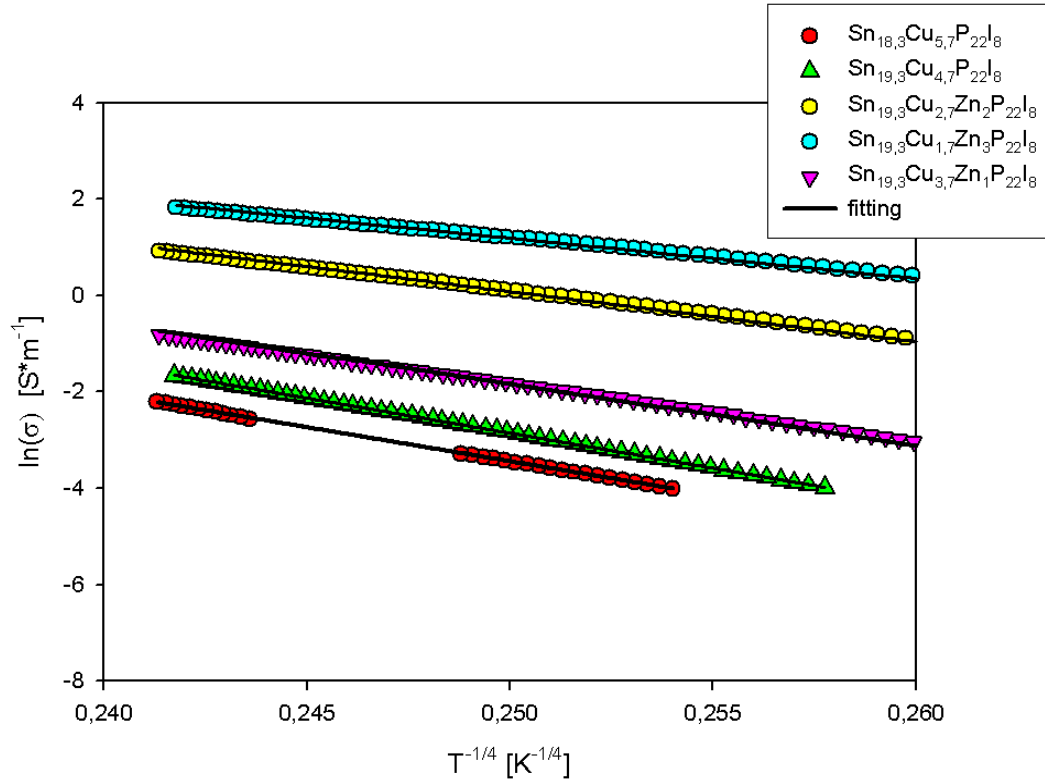


Fig. 26: Variable-range hopping behaviour found for $\text{Sn}_{18,3}\text{Cu}_{5,7}\text{P}_{22}\text{I}_8$ and $\text{Sn}_{19,3}\text{Cu}_{4,7}\text{P}_{22}\text{I}_8$, fitted with an exponent of $1/4$

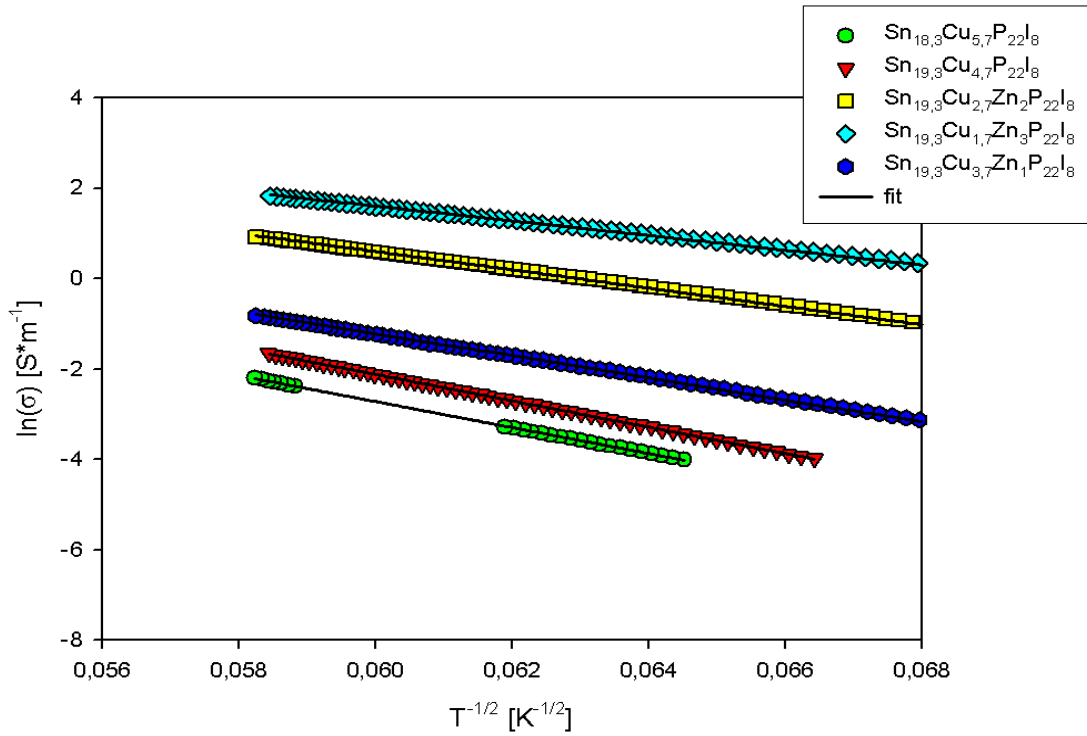


Fig. 27: Fitting of the data with an exponent of $1/2$: Here also the Zn-containing samples show a very good agreement

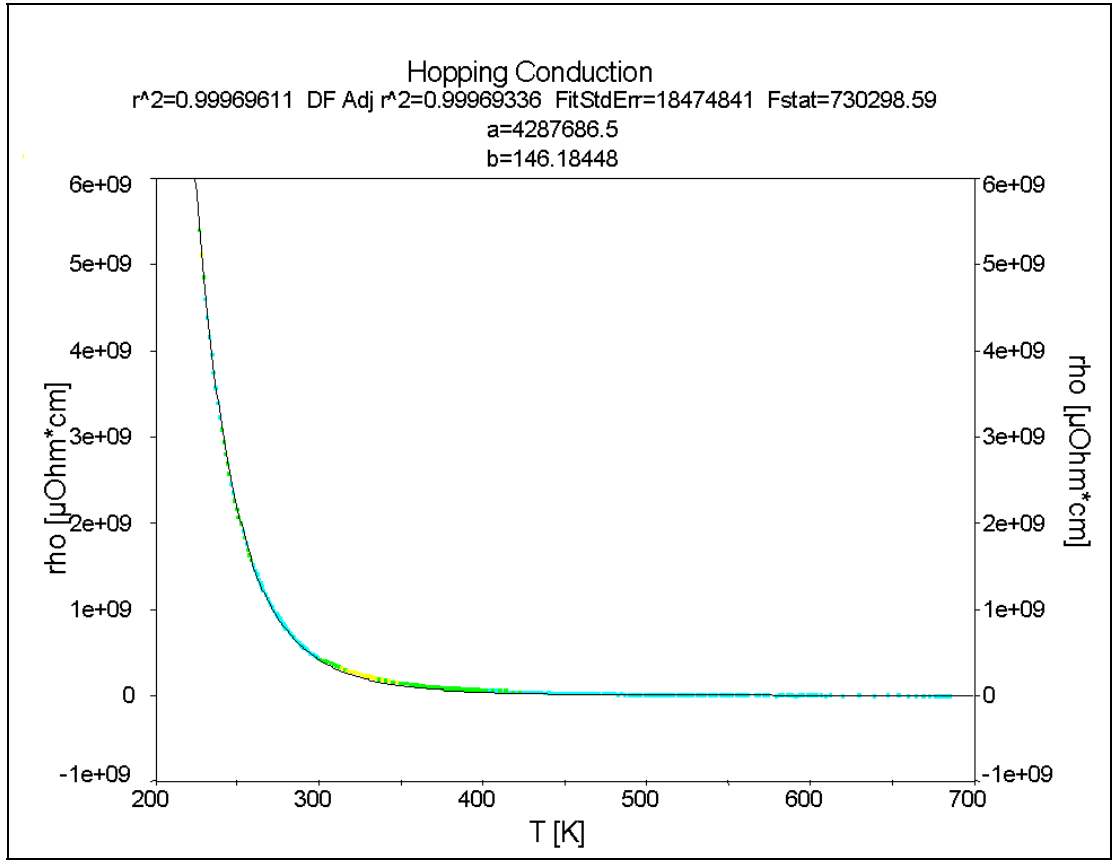


Fig. 28: Fitting of sample $\text{Sn}_{19.3}\text{Cu}_{4.7}\text{P}_{22}\text{I}_8$ in the program Table Curve, using the following equation with the free parameters a and b :

$$\rho = \frac{1}{\sigma_0 (= a)} \cdot \frac{1}{\exp\left(\frac{-T_0 (= b)}{T^{1/4}}\right)}$$

The colors of the measured points show, how good they fit to the calculated curve: starting from red (bad)-yellow-green-blue (good)

The data for the Zn-containing samples didn't fit this temperature dependency as well as the others. Especially the slope of the temperature dependency for the sample $\text{Sn}_{19.3}\text{Cu}_{1.7}\text{Zn}_3\text{P}_{22}\text{I}_8$ with the highest Zn-content couldn't be described with formula (13). Thus it seems, that by substitution of Cu by Zn, a change in the mechanism of electrical conduction was created. Although the effect of the insertion of Zn into the clathrate framework lowers the electrical resistivity, the decrease is not as high as expected. At higher temperatures the electrical resistivity drops down to $0.0129 \Omega \cdot \text{m}$ at 300°C for the compound $\text{Sn}_{19.3}\text{Cu}_{1.7}\text{Zn}_3\text{P}_{22}\text{I}_8$, but still doesn't reach a level suitable for thermoelectric applications.

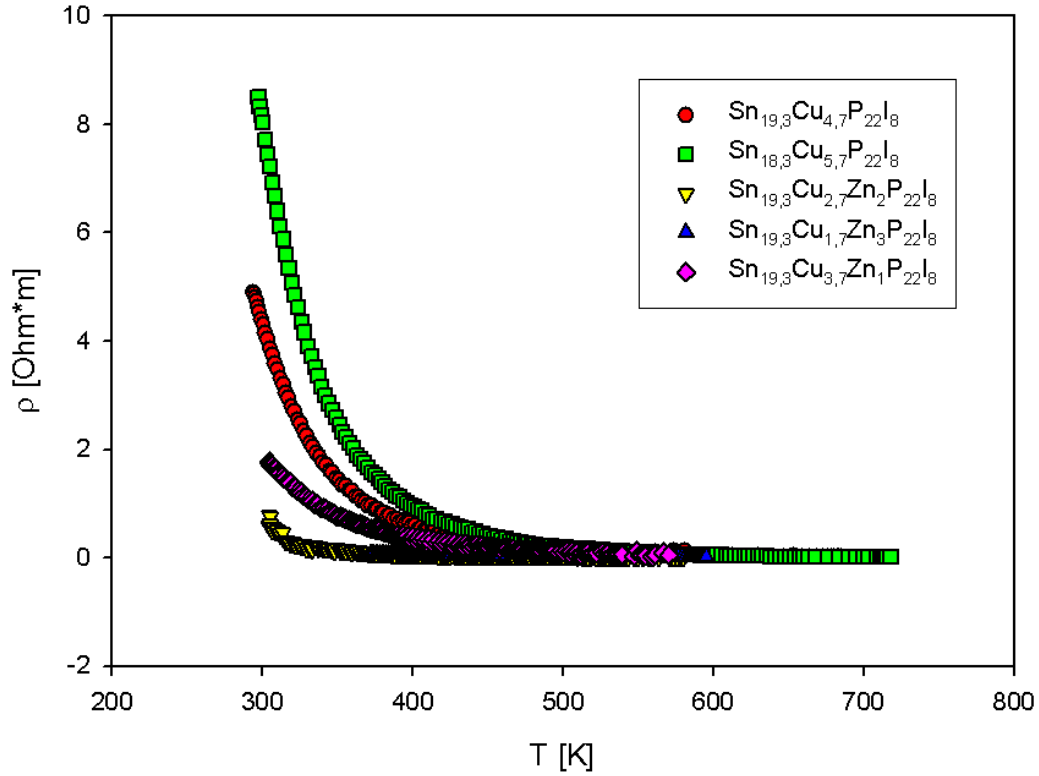


Fig. 29: Electrical resistivity of all samples except the gold and silver containing measured with the high temperature setup

For the samples containing Ag and Au the electrical resistivity was measured only in a temperature range of 290 to 590 K using the ULVAC, but the data showed a significant effect although caused by a small amount of substitution. Compared to the initial compound $\text{Sn}_{19.3}\text{Cu}_{1.7}\text{Zn}_3\text{P}_{22}\text{I}_8$ the electrical conductivity is lowered by a factor of 10^2 (Fig. 30).

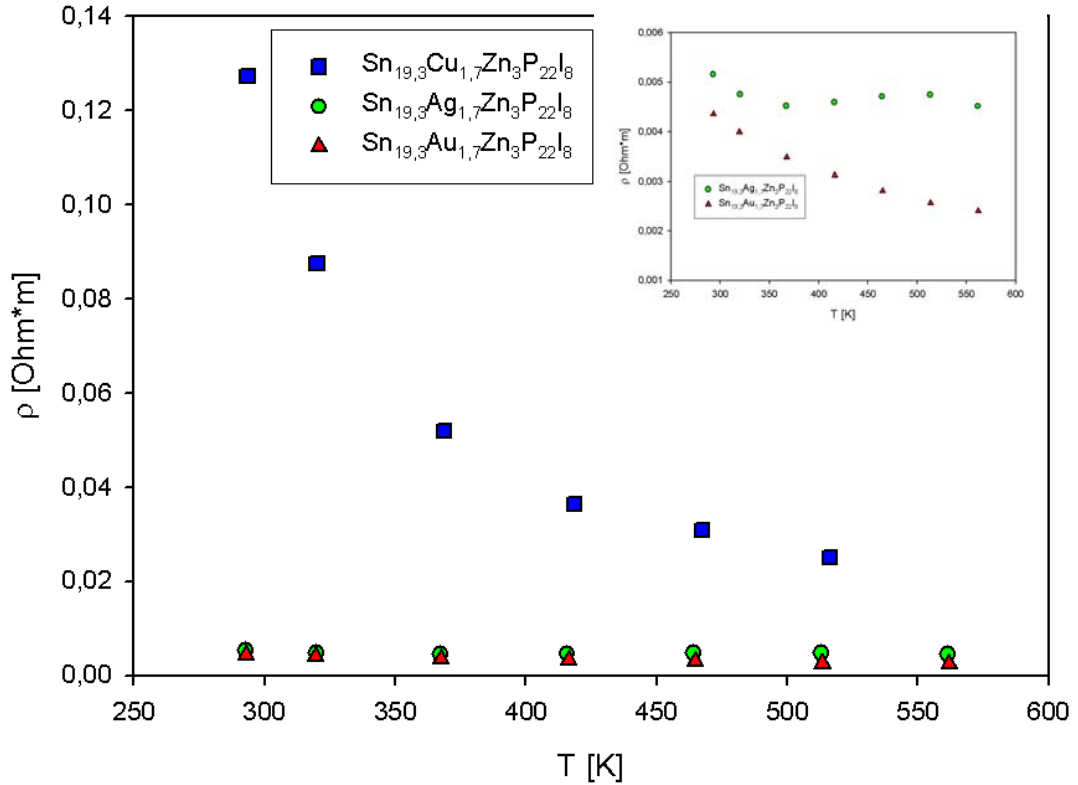


Fig. 30: Electrical resistivity of $\text{Sn}_{19.3}\text{Cu}_{1.7}\text{Zn}_3\text{P}_{22}\text{I}_8$, $\text{Sn}_{19.3}\text{Ag}_{1.7}\text{Zn}_3\text{P}_{22}\text{I}_8$ and $\text{Sn}_{19.3}\text{Au}_{1.7}\text{Zn}_3\text{P}_{22}\text{I}_8$ measured with ULVAC ZEM 3

The temperature dependence still shows a semiconducting behavior of the samples $\text{Sn}_{19.3}\text{Ag}_{1.7}\text{Zn}_3\text{P}_{22}\text{I}_8$ and $\text{Sn}_{19.3}\text{Au}_{1.7}\text{Zn}_3\text{P}_{22}\text{I}_8$.

3.2.3 Seebeck-Coefficient

The Seebeck-coefficient at temperatures below room temperature was measured only for the samples $\text{Sn}_{19.3}\text{Cu}_{1.7}\text{Zn}_3\text{P}_{22}\text{I}_8$ and $\text{Sn}_{19.3}\text{Cu}_{2.7}\text{Zn}_2\text{P}_{22}\text{I}_8$. Due to their high electrical resistivity with the available device the measurement for all the other samples was impossible. Already the values of the sample $\text{Sn}_{19.3}\text{Cu}_{2.7}\text{Zn}_2\text{P}_{22}\text{I}_8$ show a rather large scattering in the low temperature region. Thus no temperature dependency of the Seebeck-coefficient could be extracted from the measured data. The data for $\text{Sn}_{19.3}\text{Cu}_{1.7}\text{Zn}_3\text{P}_{22}\text{I}_8$ show this large scattering at temperatures lower than 150 K. At higher temperatures the Seebeck-coefficient shows a slight increase with increasing temperature.

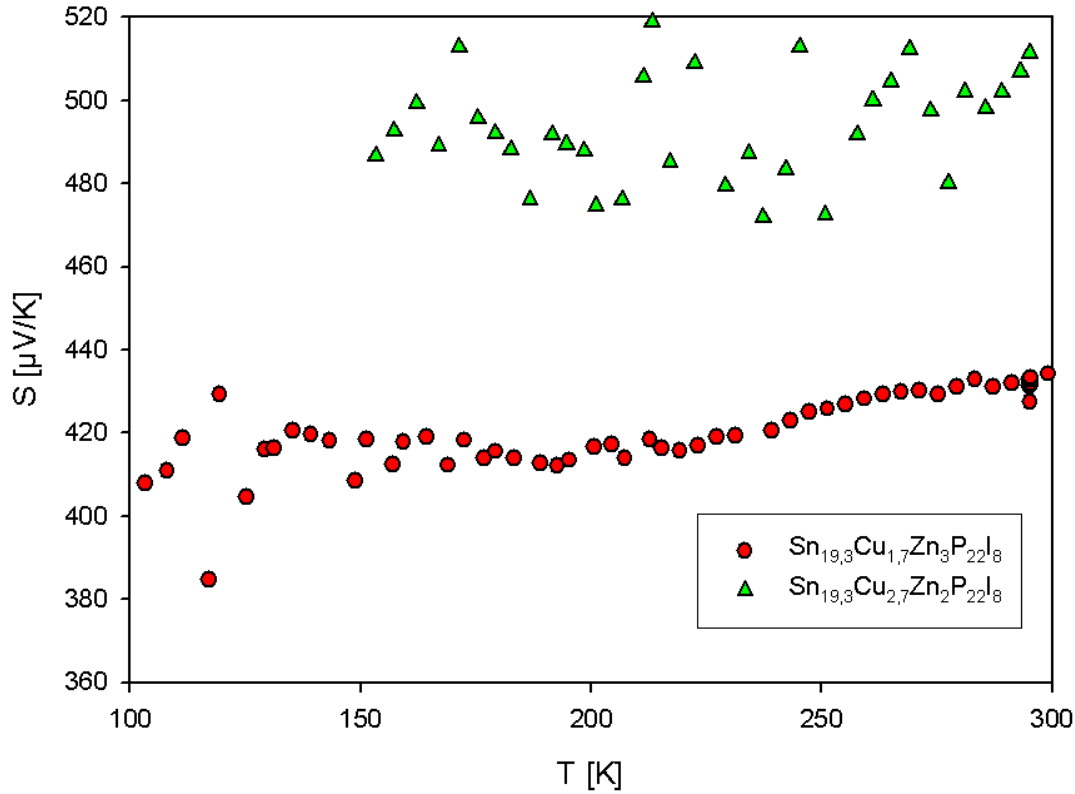


Fig. 31: Seebeck-coefficient measured below room temperature for samples $\text{Sn}_{19.3}\text{Cu}_{1.7}\text{Zn}_3\text{P}_{22}\text{I}_8$ and $\text{Sn}_{19.3}\text{Cu}_{2.7}\text{Zn}_2\text{P}_{22}\text{I}_8$

The thermopower of a material, represented by its Seebeck-coefficient, is a consequence of the movement of the charge carriers due to a temperature gradient. The resulting displacement of electrons and holes causes an electric voltage, which can be derived from the following relation:

$$(15) \quad U = S_x \cdot \nabla T$$

Here U is the resulting voltage, S_x the Seebeck-coefficient of the material x and the temperature gradient ∇T can be replaced in homogeneous materials by the temperature difference ΔT . Dependent on the free charge carriers a positive or a negative potential is created at the cold end of the gradient. Thus the Seebeck-coefficient for n-type materials is negative and for p-type materials is positive. All our samples show a positive value of S , which means they are p-doped semiconductors. Taking this find into account, which confirms the results of the structure investigations, the attempt to create an n-doped semiconductor by substituting in the clathrate framework Cu by Zn failed. Instead of the intended n-

doping the results of the structure refinement as well as the results of the investigation of the physical properties imply a p-doping. As defects may compensate the desired electron count, the general chemical formula for the Zn-containing samples should be enlarged in the following way to give a proper and complete description: $\text{Sn}_{19.3}\text{Cu}_{4.7-x}\text{Zn}_x\text{P}_{22-y}\square_y\text{I}_8$ ($x = 1, 2, 3$) where \square is a symbol for vacancies and y gives the amount of vacancies. From Rietveld refinement these vacancies could be located in the phosphorus 6d-position, which is in agreement with the so far investigated clathrate-I-compounds containing vacancies in the framework structure [18]. In the case of vacancy formation some atoms in the 24k-position become three-coordinated. It should be noted that non-standardized unit cell settings [7, 15, 18] list the 6c-site as the site with framework vacancies (6d-site in properly standardised setting!)

In the following table the amount of vacancies obtained from the Rietveld-refinement are compared to the values, which are calculated from the Zintl-formalism. In terms of the Zintl-concept the substitution of one Cu-atom by one Zn-atom produces one additional electron in the framework, which has to be compensated by the formation of vacancies. One vacancy in the 6d-position of phosphorus can compensate for 5 additional electrons. As already mentioned in 3.1.3 the vacancy formation seems to exceed the amount, which is necessary to be consistent with the Zintl-concept.

Table 8: Vacancy formation in the Zn-containing Cu-clathrates

| compound | $\text{Sn}_{19.3}\text{Cu}_{3.7}\text{Zn}_1\text{P}_{22-y}\square_y\text{I}_8$ | $\text{Sn}_{19.3}\text{Cu}_{2.7}\text{Zn}_2\text{P}_{22-y}\square_y\text{I}_8$ | $\text{Sn}_{19.3}\text{Cu}_{1.7}\text{Zn}_3\text{P}_{22-y}\square_y\text{I}_8$ |
|------------------------|--|--|--|
| y_R (Rietveld) | 0.84 | 1.14 | 2.08 |
| y_Z (Zintl) | 0.2 | 0.4 | 0.6 |
| $\Delta y = y_R - y_Z$ | 0.64 | 0.74 | 1.48 |

It seems that the created vacancies overcompensate the additional electrons coming from the Zn. The higher the Zn-content the higher is the deviation from the Zintl-concept. Nevertheless the influence on the electric resistivity is too low and furthermore the tolerance against producing vacancies in the framework seems to be already reached at the composition $\text{Sn}_{19.3}\text{Cu}_{1.7}\text{Zn}_3\text{P}_{19.2}\square_{2.8}\text{I}_8$. The silver and gold containing clathrates seem to exhibit a higher tolerance for vacancy formation, in case of Au even higher than in case of Ag. This observation is consistent with the data obtained by the measurement of electrical resistivity, because the Au-containing clathrate forms an even higher amount of vacancies in the framework. The chemical formulas $\text{Sn}_{19.3}\text{Ag}_{1.7}\text{Zn}_3\text{P}_{19.2}\square_{2.8}\text{I}_8$ and $\text{Sn}_{19.3}\text{Au}_{1.7}\text{Zn}_3\text{P}_{18.8}\square_{3.2}\text{I}_8$ show a large deviation of the Zintl-concept, which yields $y = 0.6$.

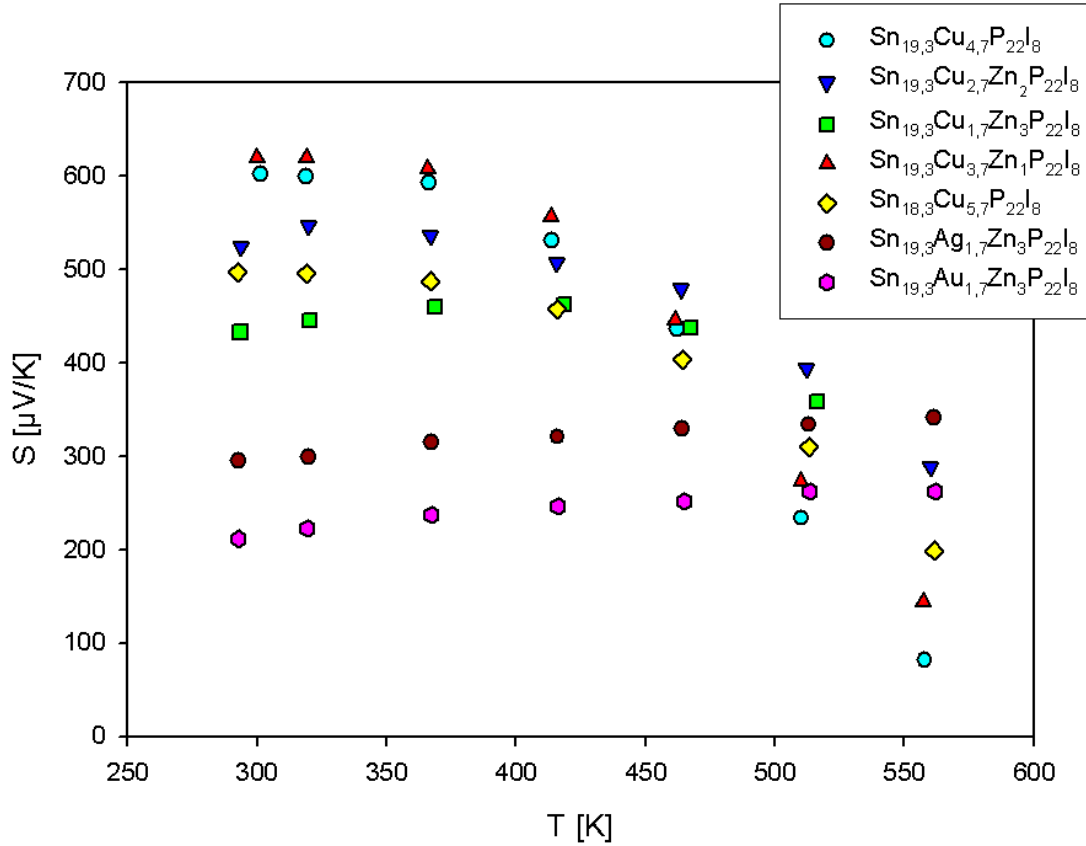


Fig. 32: Seebeck-coefficient measured with ULVAC at high temperatures

In Fig. 32 the Seebeck-coefficients at high temperatures are shown for all specimens prepared. The decrease for the Cu-containing inverse clathrates can be explained by the increase of charge carriers, which usually lowers S . At temperatures above 500 K these samples seem to exhibit metallic behaviour. The gold and silver samples do not show this behavior at 500 K. Measurements at higher temperatures will reveal further development of the S -values.

3.2.4 Thermal Conductivity

According to the PGEC-concept, mentioned in the introduction, where one material should combine thermal conductivity of a glass with electrical conductivity of a crystal, clathrates seem to be able to exhibit such a behavior. Clathrates offer a rigid structure, suitable for good electrical conductivity as well as heavy atoms rattling in cages of this structure leading to a lower thermal conductivity due to additional scattering of phonons. In the inverse clathrates a four-bonded network is built, usually formed by silicon, germanium, tin, phosphorus, arsenic or antimony, which provides large cages filled with electronegative elements. There are no rigid bonds between the framework and the guests. Thus the guest atoms can serve as sufficient rattlers for the phononic part of the thermal conductivity. At room temperature the heat conductivity

of many type-I-clathrates is $0.5\text{--}1.5 \text{ Wm}^{-1}\text{K}^{-1}$, which is comparable to that of amorphous compounds. Calculations for clathrate compounds based on the Wiedemann-Franz law demonstrated that the electronic component of the heat conductivity is not higher than 6–8 %. Consequently, the heat conductivity in these materials is dominated by the contribution of the lattice, which is efficiently lowered by the rattling of the loosely bonded guest atoms. This mechanism is evidenced also by a slight decrease in the heat conductivity of most clathrates with decreasing temperature, which corresponds to a decrease in vibration amplitudes of the guest atoms [18]. The resulting thermal conductivity depends on factors like the guest atom size and mass, the host-guest size matching, and the possibility that guest atoms of different kind can be alternated in the framework cages. In the general case, the thermal conductivity decreases as the guest atom mass and the volume free for its oscillations increase, and with the increase in the degree of disordering in the distribution of two different guest atoms [17].

Iodine, the heaviest anionic guest, which can be incorporated into a clathrate compound, was used for my samples. Although only the thermal conductivity of the samples $\text{Sn}_{19.3}\text{Cu}_{1.7}\text{Zn}_3\text{P}_{22}\text{I}_8$ and $\text{Sn}_{19.3}\text{Cu}_{2.7}\text{Zn}_2\text{P}_{22}\text{I}_8$ was investigated, their thermal conductivity is found to be in the expected order of magnitude.

$\text{Sn}_{19.3}\text{Cu}_{1.7}\text{Zn}_3\text{P}_{22}\text{I}_8$ was measured with the low temperature equipment as well as with the high temperature equipment of the flash line. The thermal conductivity of $\text{Sn}_{19.3}\text{Cu}_{2.7}\text{Zn}_2\text{P}_{22}\text{I}_8$ was only measured at high temperatures. The reason why it shows a significant lower thermal conductivity compared to the values obtained for $\text{Sn}_{19.3}\text{Cu}_{1.7}\text{Zn}_3\text{P}_{22}\text{I}_8$ remains unclear. An increase of the electronic contribution cannot explain this difference.

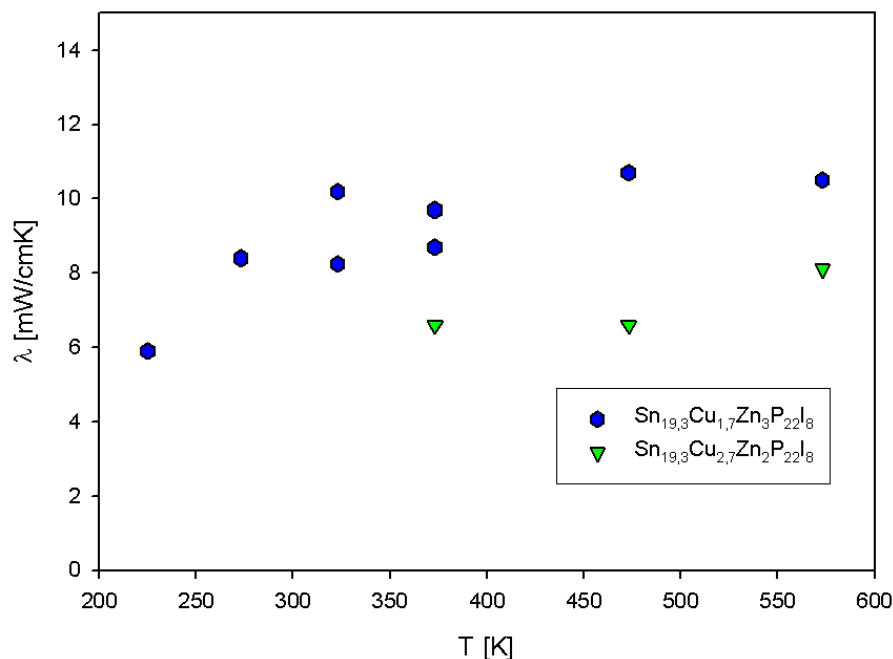


Fig. 33: Thermal conductivity of the samples $\text{Sn}_{19.3}\text{Cu}_{1.7}\text{Zn}_3\text{P}_{22}\text{I}_8$ and $\text{Sn}_{19.3}\text{Cu}_{2.7}\text{Zn}_2\text{P}_{22}\text{I}_8$

3.2.5 ZT-Figure of Merit

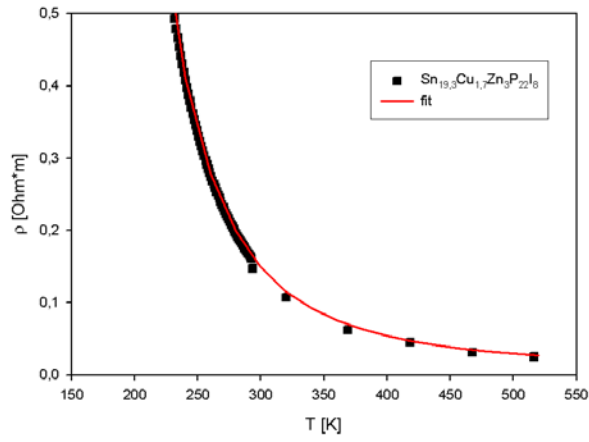
The thermoelectric figure of merit was calculated for the samples $\text{Sn}_{19.3}\text{Cu}_{1.7}\text{Zn}_3\text{P}_{22}\text{I}_8$ and $\text{Sn}_{19.3}\text{Cu}_{2.7}\text{Zn}_2\text{P}_{22}\text{I}_8$. Equation (1) is used to calculate this dimensionless quantity:

$$(1) \quad Z \cdot T = \frac{T \cdot S^2}{\kappa \cdot \rho}$$

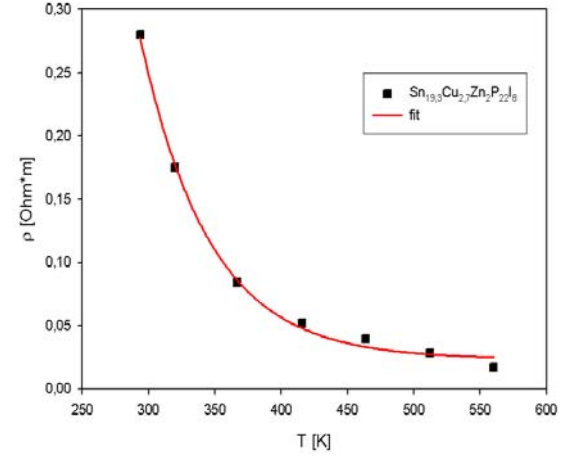
The values for the ZT, of course, are too small by more than two orders of magnitude for practical applications. Although the thermal conductivity is at a good level and the Seebeck-coefficient is very high, the poor electrical conductivity diminishes the figure of merit to these very low values.

The results for the silver and gold sample are quite promising and should increase ZT significantly, when the thermal conductivity stays at the same level, which due to the clathrate structure and the incorporation of heavier atoms should in principle be the case.

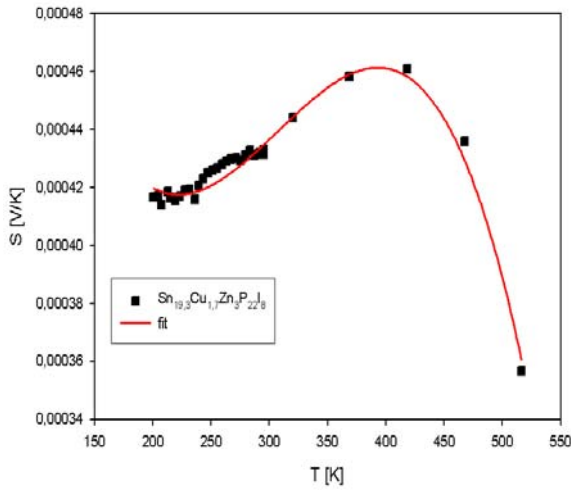
To calculate the ZT-dependence on temperature, values of the three physical properties electrical resistivity, Seebeck-coefficient and thermal conductivity need to be at the same temperature. Thus a suitable regression was applied to the measured data. For the electrical resistivity the fitted curves were used, for all the other data linear or cubic polynomial regression was used (Fig. 34).



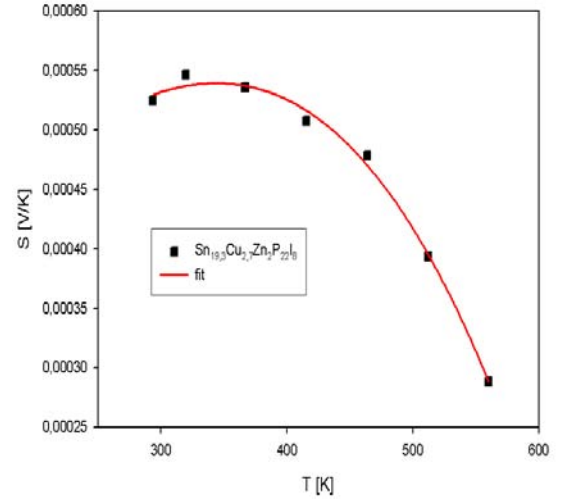
a: Electrical resistivity+fit of $\text{Sn}_{19.3}\text{Cu}_{1.7}\text{Zn}_3\text{P}_{22}\text{I}_8$



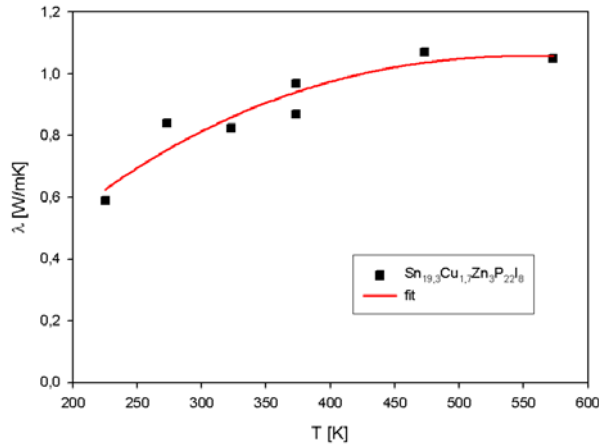
b: Electrical resistivity+fit of $\text{Sn}_{19.3}\text{Cu}_{2.7}\text{Zn}_2\text{P}_{22}\text{I}_8$



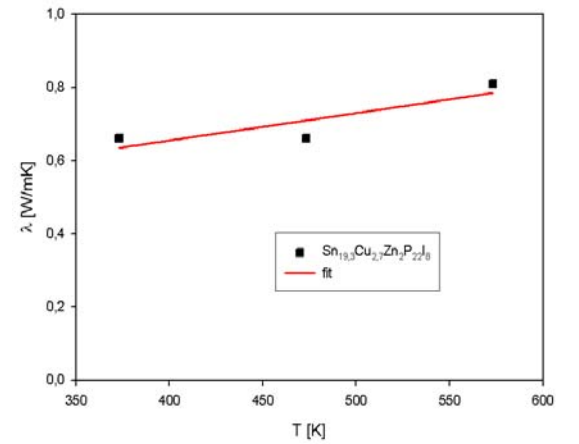
c: Seebeck-coefficient of $\text{Sn}_{19.3}\text{Cu}_{1.7}\text{Zn}_3\text{P}_{22}\text{I}_8$



d: Seebeck-coefficient of $\text{Sn}_{19.3}\text{Cu}_{2.7}\text{Zn}_2\text{P}_{22}\text{I}_8$



e: Thermal conductivity of $\text{Sn}_{19.3}\text{Cu}_{1.7}\text{Zn}_3\text{P}_{22}\text{I}_8$



f: Thermal conductivity of $\text{Sn}_{19.3}\text{Cu}_{2.7}\text{Zn}_2\text{P}_{22}\text{I}_8$

Fig. 34: Data and regression function used for the calculation of ZT

For the samples $\text{Sn}_{19,3}\text{Ag}_{1,7}\text{Zn}_3\text{P}_{22}\text{I}_8$ and $\text{Sn}_{19,3}\text{Au}_{1,7}\text{Zn}_3\text{P}_{22}\text{I}_8$ the thermal conductivity values were estimated using an average value of the measured data of the samples $\text{Sn}_{19,3}\text{Cu}_{1,7}\text{Zn}_3\text{P}_{22}\text{I}_8$ and $\text{Sn}_{19,3}\text{Cu}_{2,7}\text{Zn}_2\text{P}_{22}\text{I}_8$.

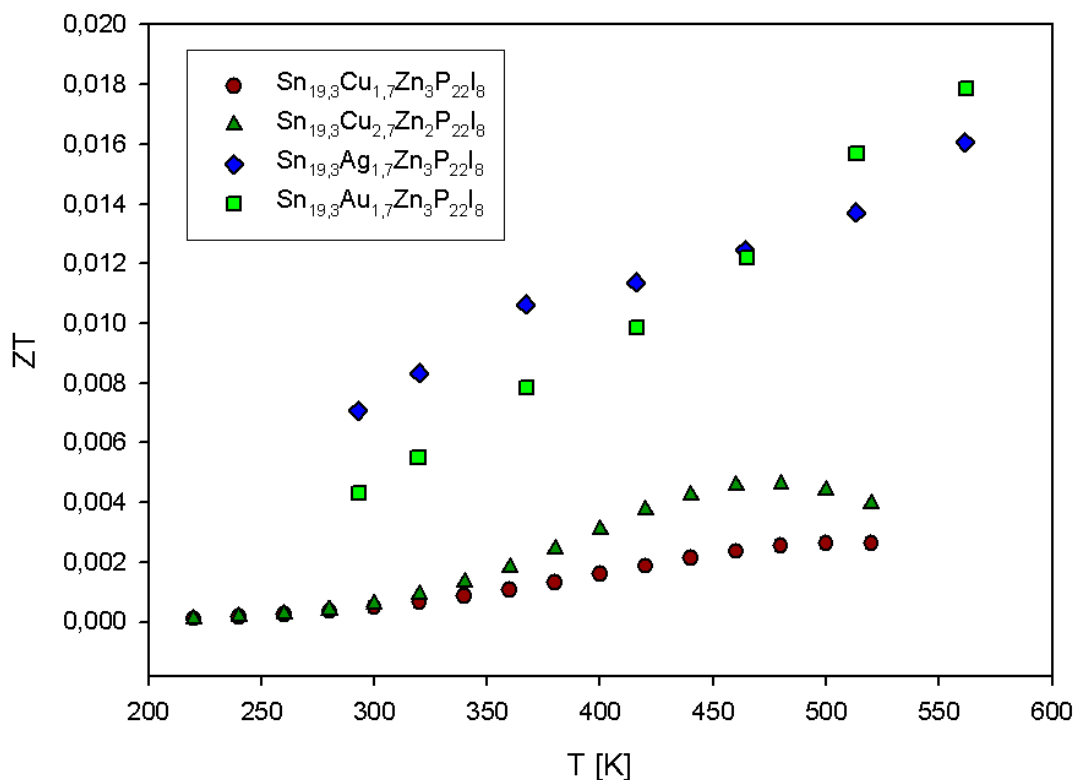


Fig. 35: Thermoelectric figure of merit ZT of $\text{Sn}_{19,3}\text{Cu}_{1,7}\text{Zn}_3\text{P}_{22}\text{I}_8$, $\text{Sn}_{19,3}\text{Cu}_{2,7}\text{Zn}_2\text{P}_{22}\text{I}_8$, $\text{Sn}_{19,3}\text{Ag}_{1,7}\text{Zn}_3\text{P}_{22}\text{I}_8$ and $\text{Sn}_{19,3}\text{Au}_{1,7}\text{Zn}_3\text{P}_{22}\text{I}_8$

The ZT -value for both, $\text{Sn}_{19,3}\text{Cu}_{1,7}\text{Zn}_3\text{P}_{22}\text{I}_8$ and $\text{Sn}_{19,3}\text{Cu}_{2,7}\text{Zn}_2\text{P}_{22}\text{I}_8$, increases keenly with temperature, but reaches a maximum in-between 450 and 500 K and reduces again at higher temperatures, because of the diminishment of the Seebeck-coefficient. At high temperatures the electrical resistivity of semiconductors decreases only slightly and thus S , which enters ZT as S^2 , dominates the further development of the figure of merit. Due to the lower electrical resistivity the ZT -values of the silver and gold-containing clathrates is increased significantly. Furthermore at temperatures above 500 K still no maximum appears. Although the compounds still need an improvement of the ZT -values by a factor of at least 50 to reach the region interesting for thermoelectric applications.

3.3 Mechanical Properties

For practical applications and an economical utilization besides the thermoelectric properties, which of course are the basic requirements, also the mechanical properties of the thermoelectric materials play a decisive role. For example to be interesting for use in the automotive industry the materials should show a certain mechanical resistance. Up to now the investigations on mechanical properties of possible new

thermoelectric materials were disregarded and nothing is known and published on the mechanical performance of inverse clathrates.

To get a first indication on the elastic properties the shear modulus of one sample was measured.

As already explained in 2.9 a special method was used to get a sample of suitable size. Because of the preparation method the density of the clathrate-I-type $\text{Sn}_{19.3}\text{Cu}_{4.7}\text{P}_{22}\text{I}_8$ reached only 87 % of the theoretical density. The grain size of this sample was somehow larger than that of all other samples.

The highest value of shear modulus of 8.5 GPa was measured at $-130\text{ }^\circ\text{C}$ and an almost linear decrease to a G-value of 4.9 GPa at $250\text{ }^\circ\text{C}$ of the shear modulus with increasing temperature was observed. The slightly different slopes from low temperatures to room temperature and from room temperature to the maximum temperature might stem from the exchange of the equipment. At room temperature (295 K) a G-value of 6.7 GPa was observed, which is quite low compared to the value of 44.7 GPa in the case of for example copper metal. The temperature dependency of the shear modulus of $\text{Sn}_{19.3}\text{Cu}_{4.7}\text{P}_{22}\text{I}_8$ is quite large. Due to the brittleness of the material the sample was fixed very carefully, however, was not anchored very firmly in the rheometer, which caused some problems during the measurement.

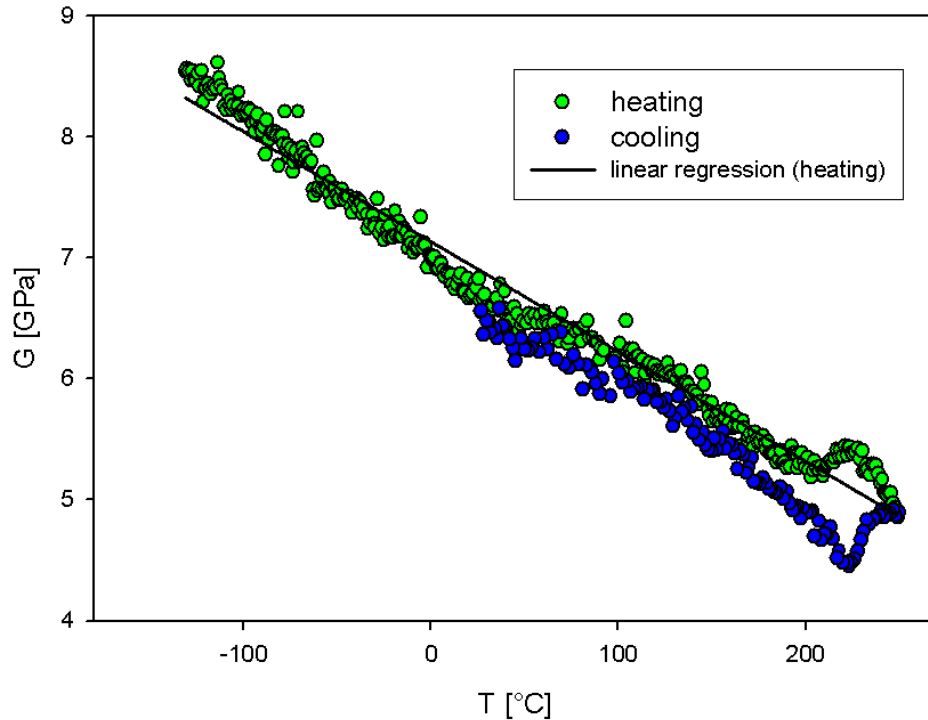


Fig. 36: Shear modulus of $\text{Sn}_{19.3}\text{Cu}_{4.7}\text{P}_{22}\text{I}_8$: the green points belong to measurement during heating and the blue points belong to the measurement during cooling

Above $200\text{ }^\circ\text{C}$ a small effect can be seen, which could indicate a phase transition, but to confirm this more measurements have to be done.

4. Conclusion

For the already known and published clathrate-I-compound $\text{Sn}_{19.3}\text{Cu}_{4.7}\text{P}_{22}\text{I}_8$ a faster synthesis method using ball mill and hot press was found, which furthermore offers the opportunity of producing suitable compact shapes to investigate the thermoelectric properties of the material. The thermoelectric measurements confirmed that $\text{Sn}_{19.3}\text{Cu}_{4.7}\text{P}_{22}\text{I}_8$ is a narrow-gap semiconductor as expected according to the Zintl-concept. Thus various substitutions were performed in order to tailor the thermoelectric properties. The successful substitution of Cu by Zn yielded a significant increase of the lattice parameter. The measurement of electrical resistivity and Seebeck-coefficient manifested, that the primary attempt to incorporate additional electrons into the clathrate-framework failed. Rietveld-analysis of the powder diffraction patterns revealed the formation of vacancies in the 6d-site jointly occupied by phosphorus. The systematic increase of the total number of vacancies in the framework with increase of the Zn-content can explain the reduction of electric resistivity as well as a simultaneous decline of Seebeck-coefficient. Furthermore the positive sign of S confirms the p-doping in $\text{Sn}_{19.3}\text{Cu}_{4.7-x}\text{Zn}_x\text{P}_{22}\text{I}_8$. Although the thermal conductivity values indicate a glass-like behavior, which is typically observed for clathrate-I-structures, the thermoelectric figure of merit is too low due to the still very high electrical resistivity.

The attempt to incorporate Ag and Au, with the combined synthesis method of ball mill and hot press was successful and led to the discovery of two novel inverse clathrates, $\text{Sn}_{19.3}\text{Ag}_{1.7}\text{Zn}_3\text{P}_{19.2}\square_{2.8}\text{I}_8$ and $\text{Sn}_{19.3}\text{Au}_{1.7}\text{Zn}_3\text{P}_{18.8}\square_{3.2}\text{I}_8$. The values of electrical conductivity as well as the values of the Seebeck-coefficient are promising for future investigations on inverse clathrates containing Ag or Au in the framework and further increase of the Ag or Au-amount in the host-framework may lead to a further improvement of the thermoelectric properties.

A first measurement on elastic properties of an inverse clathrate, $\text{Sn}_{19.3}\text{Cu}_{4.7}\text{P}_{22}\text{I}_8$, was done which especially for economical applications play a decisive role,.

The periodic table still has a lot of elements in store for the incorporation into the framework of inverse clathrate components and for many of the so far synthesised and published inverse clathrates no thermoelectric properties have been investigated. In this as well as in other works [7, 10, 12] it was shown, that the variation of the composition could significantly change the physical properties, particularly when the compounds constitution deviates from the Zintl-concept.

References:

- [1] Menke, H.; Von Schnering, H. G., Zeitschrift fuer Anorganische und Allgemeine Chemie (1973), 395(2-3), 223-38
- [2] Chu, T. L.; Chu, S. S.; Ray, R. L., Journal of Applied Physics (1982), 53(10), 7102-3
- [3] Shatruk, M. M.; Kovnir, K. A.; Shevelkov, A. V.; Presniakov, I. A.; Popovkin, B. A., Inorganic Chemistry (1999), 38(15), 3455-3457
- [4] Shatruk, M. M.; Kovnir, K. A.; Lindsjoe, M.; Presniakov, I. A.; Kloo, L. A.; Shevelkov, A. V., Journal of Solid State Chemistry (2001), 161(2), 233-242
- [5] Reny, E.; Yamanaka, S.; Cros, C.; Pouchard, M., AIP Conference Proceedings (2001), 590(Nanonetwork Materials), 499-502
- [6] Kovnir, K. A.; Zaikina, J. V.; Reshetova, L. N.; Olenov, A. V.; Dikarev, E. V.; Shevelkov, A. V., Inorganic Chemistry (2004), 43(10), 3230-3236
- [7] Kovnir, K. A.; Shatruk, M. M.; Reshetova, L. N.; Presniakov, I. A.; Dikarev, E. V.; Baitinger, M.; Haarmann, F.; Schnelle, W.; Baenitz, M.; Grin, Y.; Shevelkov, A. V., Solid State Sciences (2005), 7(8), 957-968
- [8] Kishimoto, K.; Arimura, S.; Koyanagi, T.; Applied Physics Letters (2006), 88(22), 222115/1-222115/3
- [9] Kishimoto, K.; Akai, K.; Muraoka, N.; Koyanagi, T.; Matsuura, M.; Applied Physics Letters (2006), 89(17), 172106/1-172106/3
- [10] Kishimoto, K.; Koyanagi, T.; Akai, K.; Matsuura, M.; Japanese Journal of Applied Physics, Part 2: Letters & Express Letters (2007), 46(29-32), L746-L748
- [11] Zaikina, J. V.; Kovnir, K. A.; Schwarz, U.; Borrmann, H.; Shevelkov, A. V., Zeitschrift fuer Kristallographie - New Crystal Structures (2007), 222(3), 177-179
- [12] Zaikina, J. V.; Schnelle, W.; Kovnir, K. A.; Olenov, A. V.; Grin, Y.; Shevelkov, A. V., Solid State Sciences (2007), 9(8), 664-671
- [13] Zaikina, J. V.; Kovnir, K. A.; Sobolev, A. V.; Presniakov, I. A.; Prots, Y.; Baitinger, M.; Schnelle, W.; Olenov, A. V.; Lebedev, O. I.; Van Tendeloo, G.; Grin, Y.; Shevelkov, A. V., Chemistry (Weinheim an der Bergstrasse, Germany) (2007), 13(18), 5090-9

- [14] Kovnir, K. A.; Sobolev, A. V.; Presniakov, I. A.; Lebedev, O. I.; Van Tendeloo, G.; Schnelle, W.; Grin, Y.; Shevelkov, A. V., *Inorganic Chemistry* (2005), 44(24), 8786-8793
- [15] Shatruk, M. M.; Kovnir, K. A.; Shevel'kov, A. V.; Popovkin, B. A., *Zhurnal Neorganicheskoi Khimii* (2000), 45(2), 203-209
- [16] Kovnir, K. A.; Abramchuk, N. S.; Zaikina, J. V.; Baitinger, M.; Burkhardt, U.; Schnelle, W.; Olenov, A. V.; Lebedev, O. I.; Van Tendeloo, G.; Dikarev, E. V.; Shevelkov, A. V., *Zeitschrift fuer Kristallographie* (2006), 221(5-7), 527-532
- [17] Shevelkov A. V., *Russian Chemical Reviews* (2008), 77(1), 1-19
- [18] Kovnir K. A., Shevelkov A. V., *Russian Chemical Reviews* (2004), 73(9), 923-938
- [19] Mott, N. F., *Phil Mag.* B19, 835(1984)
Mott, N. F., *The Physics of Hydrogenated Amorphous Silicon* Vol. II. ed. by J. D. Joannopoulos and G. Luckowsky, *Topics in Applied Physics*, Vol. 56(Springer, Berlin Heidelberg 1984), p. 169
- [20] Parthé, E.; Gelato, L.; Chabot, B.; Penzo, M.; Cenxual, K.; Gladyshevskii, R., *TYPIX standardized data and crystal chemical characterization of inorganic structure types* (Berlin: Springer) 1994.
- [21] Villars, P.; Prince, A.; Okamoto, H., *Handbook of Ternary Alloy Phase Diagrams*, Vol. 8 (1995)
- [22] Rogl, P.; *Formation of Clathrates. in Handbook on Thermoelectrics*, M. Rowe (ed.); RCR 2005, pp.26
- [23] Mudryk Ya.; Rogl P.; Paul C.; Berger S.; Bauer E.; Hilscher G.; Godart C.; Noel H.-J., *J. Phys.: Condens. Matter* (2002), 14, 7991-8004
- [24] Rodriguez-Carvajal J. FULLPROF: A Program for Rietveld Refinement and Pattern Matching Analysis. see also *Physica B*, (1993);192, 55
- [25] Roisnel, T.; Rodriguez-Carvajal, J., *Materials-Science-Forum* 378-381 (2001) 118-123.
- [26] Kauzlarich M. S. (Ed.), *Chemistry, Structure and Bonding of Zintl Phases and Ions*. New York: VCH, (1996)
- [27] Zintl, E.; Woltersdorf, G., *Zeitschrift fuer Elektrochemie und Angewandte Physikalische Chemie* (1935), 41 876-9

- [28] Eurotherm User Manual, TE10S Solid State Relay, (1996), 8
- [29] Suryanarayana, C., Progress in Materials Science (2001), 46, 1-184
- [30] FCT Systeme GmbH, Betriebsanleitung: Heisspresse(2006)
- [31] Spieß, L.; Schwarzer, R.; Behnken, H.; Teichert, G.; Moderne Röntgenbeugung: Röntgendiffraktometrie für Materialwissenschaftler, Physiker und Chemiker,(2005), Vieweg + Teubner Verlag
- [32] Allmann, R.; Röntgenpulverdiffraktometrie: Rechnergestützte Auswertung, Phasenanalyse und Strukturbestimmung, (2003), Springer-Verlag
- [33] User Manual of ULVAC, ZEM 3 (2008)

Acknowledgments

First of all I want to express my deep gratitude to Prof. P. F. Rogl for his guidance and constant support of the whole research work. I'm very thankful for the help concerning all questions to theoretical and experimental details.

Furthermore I need to thank all the members of the group "Funktionelle Materialien" for their kind introduction to all experimental techniques and their incessant support for all kind of questions.

Great appreciation also belongs to Prof. E. Bauer and his group at the TU Wien, for giving me not only the opportunity to do the measurements of physical properties of my samples, but also explained the equipment to me and helped me using it.

Special thanks I also want to give to Mag. Marius Reinecker, member of the group "Nichtlineare Physik" at the Universität Wien, for doing the elastic property measurements and the detailed discussion of the results.

I very gratefully acknowledge financial support by the BMfVIT-FFG within the project "THEKLA".

Curriculum Vitae

Geboren: 26. 02. 1983, Wien

Vater: Erich Falmbigl, Bankangestellter

Mutter: Christiane Falmbigl, Ergotherapeutin

Schulbildung: Volksschule: 1989- 1993 Volksschule Mistelbach
Gymnasium: 1993- 2001 Bundesgymnasium Laa/Thaya

Präsenzdienst: 09. 2001- 05. 2002 Bolfraskaserne Mistelbach

Studium: Studienrichtung Chemie seit 10. 2002 an der Universität Wien